國立臺灣大學理學院物理學系

碩士論文

Department of Physics

College of Science

National Taiwan University

Master Thesis

論四維共形反常下的量子黑洞

On Quantum Black Holes with 4D Weyl Anomaly

廖根逸

Keng-Yi Liao

指導教授：賀培銘 博士

川合光 博士

Advisor: Pei-Ming Ho, Ph.D.

Hikaru Kawai, Ph.D.

中華民國 112 年 07 月

July 2023

doi:10.6342/NTU202302515

國立臺灣大學碩士學位論文
口試委員會審定書
MASTER'S THESIS ACCEPTANCE CERTIFICATE
NATIONAL TAIWAN UNIVERSITY

（論文中文題目）(Chinese title of Master's thesis)

論四維共形反常下的量子黑洞.

（論文英文題目）(English title of Master's thesis)

On Quantum Black Holes with 4D Weyl Anomaly

本論文係 廖根遠 (姓名) R10222057 （學號）在國立臺灣大學 物理 (系/所/學位學程)完成之碩士學位論文，於民國 112 年 07 月 18 日承下列考試委員審查通過及口試及格，特此證明。

The undersigned, appointed by the Department / Institute of Physics on 18 (date) 07 (month) 2023 (year) have examined a Master's thesis entitled above presented by LIAO, KEN-YU (name) R10222057 (student ID) candidate and hereby certify that it is worthy of acceptance.

口試委員 Oral examination committee:

高涌泉		
（指導教授 Advisor）		
陳順華	太田信義	
川合一光		

系主任/所長 Director:

doi:10.6342/NTU202302515

誌謝

在就讀台灣大學物理系研究所的期間，我接受到許多人的幫助與鼓勵。因此我希望在此表達我最大的感謝之意。尤其這篇論文內容的合作者：賀培銘教授、川合光教授與橫倉祐貴博士。在物理所弦論組學習、研究的期間，賀培銘教授、川合光教授、黃宇廷教授、陳恆榆教授與 801 的各位同學給予我許多建議、協助等，才能使得我成長並順利完成此論文。同時，我也希望能感謝父母親與家人的支持與鼓勵，才能讓我完成學業。雖然只是簡短的幾句話，但是我希望能以此表達我無盡的感謝。

2023.07

doi:10.6342/NTU202302515

摘要

我們考慮半經典愛因斯坦方程式下的共形物質場，並研究四維球對稱靜態黑洞的內部幾何結構。通過假設一個狀態方程和考慮四維共形反常，我們解愛因斯坦方程式的跡，因為它是與幾何和量子態無關。我們透過兩個步驟分析了解空間的全局結構。首先，我們在解空間中確定了 3 個漸近解和它們的局部行為。然後，我們通過數值求解全局結構來確定隨著 r 增加解空間內的流動。在獲得我們了解解空間的完整行為之後，我們加入物理邊界條件，並展示了黑洞的普遍結構，包括黑洞表面附近近普朗克曲率的密集部分和底部的殼層結構。表面下的殼層結構提供了各種可能的型態。同時，透過我們的模型，我們可以確定黑洞內部型態變化的最小長度。以此為基礎，我們計算出，因為這個結構的存在，使得熵的形式與黑洞熵符合。此外，我們也給出證據證明此結構的不是靜止的。

關鍵字：黑洞、共形物質場、共形異常、黑洞熵、半古典愛因斯坦方程

doi:10.6342/NTU202302515

Abstract

We consider the semi-classical Einstein equation for conformal matter fields and mainly study the interior geometry of 4D spherical static black holes. By adopting an equation of state and 4D Weyl anomaly, we solve the trace of the Einstein equation, which is geometric and state independent. We analyze the solution space in two steps. First, we identify 3 asymptotic solutions and their local behaviors in the solution space. Then, we numerically find the transition between those asymptotic solutions. After obtaining a full picture of the solution space of our setup, we then apply the physical boundary conditions, and show some possible structures of black holes, which consists of a dense part with near-Planckian curvatures at the surface and shell structures beneath. The shell structure below the surface provides a variety patterns. By considering the most probable set of patterns, we recover the entropy area law. In addition, we also show that the internal structures are time dependent.

doi:10.6342/NTU202302515

Keyword: Black Hole, Conformal Matter Field, Weyl Anomaly, Entropy, Semi-classical Einstein Equation.

doi:10.6342/NTU202302515

Content

doi:10.6342/NTU202302515

doi:10.6342/NTU202302515

List of Plots

doi:10.6342/NTU202302515

doi:10.6342/NTU202302515

Chapter 1

Introduction

To find the correct path toward quantum gravity, researchers have been studying in details about quantum field theory in curved backgrounds [1–4]. That is how spacetime can influence quantum fields. On the other hand, general relativity tells us that matter and spacetime are in a dynamical relation through Einstein equation [5]. That suggests a consistent quantum theory must also satisfy the other direction, that is, quantum fields can have impact on spacetime (or geometry) [6–12].

Hawking radiation is one of the nontrivial consequence when we talk about quantum field theory in curved spacetime [1,13]. Take Schwarzschild black hole in 4 dimensional spacetime for example, which has the metric

$$ds^2 = -\left(1 - \frac{a_0}{r}\right) dt^2 + \left(1 - \frac{a_0}{r}\right)^{-1} dr^2 + r^2 d\Omega_2. \tag{1.0.1}$$

This metric has a fictitious singularity at $r = a$. That means this is only due to the limit of chosen coordinate system, and the region is nothing more than empty space [4]. However, this description only applies when we consider classical physics. As pointed out by Hawking, the region near horizon is not exactly vacuum from a distant observer's viewpoint [1]. This

doi:10.6342/NTU202302515

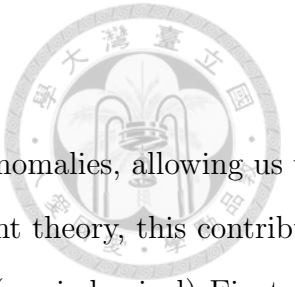

nontrivial contribution can be understood as cancellation of Weyl anomalies, allowing us to consider it in terms of energy momentum tensor [14]. As a consistent theory, this contribution can set some corrections on the spacetime geometry through (semi-classical) Einstein equation.

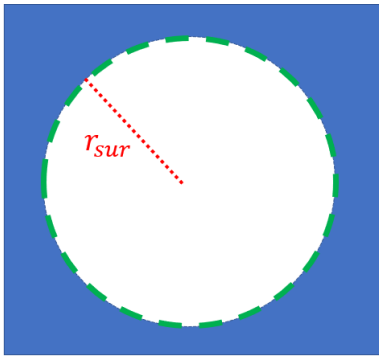

Figure 1.1: A graph to show the considered system in configuration space.

In this thesis, we are going to consider an uncharged, rotationless black hole in a 4 dimensional spherically symmetric universe. As we have mentioned above, we can classify the universe into 2 regions depending on whether quantum effects, such as vacuum polarization and particle creations, are important. We place the black hole at the center of our coordinate systems, and split the universe into white and blue regions shown in Fig. 1.1. In the figure, the center is assumed to coincide with the white region, and the separation is identified at $r = r_{sur}$ where the subscript will be clearer later in Sec. 6.2.

Within the blue region, we assume quantum effects are small, and the region can be well-approximated by the Schwarzschild metric, Eq. (1.0.1). On the other hand, in the white region, we assume quantum effects cannot be neglected, and its size should be similar to that of the black hole, according to Hawking. In there, we treat it consistently with a semi-classical approach. That is, we assume the matter building up the black hole is well-described by a theory consists of N quantum fields, which are quantized under curved spacetime, and are consistent with semi-classical Einstein equation.

doi:10.6342/NTU202302515

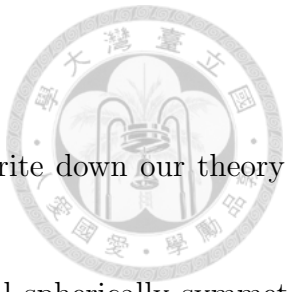

After having a full picture to what we are exploring in, let's write down our theory in terms of an effective field theory.

First, for the metric inside r_{sur}, since we are in a 4 dimensional spherically symmetric spacetime, the most general ansatz is

$$ds^2 = -\left(1 - \frac{a(t,r)}{r}\right) e^{A(t,r)} dt^2 + \frac{1}{1 - \frac{a(t,r)}{r}} dr^2 + r^2 d\Omega_2. \tag{1.0.2}$$

Note that since we are not connecting to asymptotic flat region, the metric will not be fixed to Schwarzschild metric [4]. It would be great if we are able to solve the semi-classical Einstein equation with this metric, but it is in general a highly complicated task. Therefore, in this paper, we mainly focus on solving the static case, that is,

$$ds^2 = -\left(1 - \frac{a(r)}{r}\right) e^{A(r)} dt^2 + \frac{1}{1 - \frac{a(r)}{r}} dr^2 + r^2 d\Omega_2, \tag{1.0.3}$$

and discuss the time dependent case latter.

The physics in $r \leq r_{sur}$, as mentioned above, is described by semi-classical Einstein equation, which is our equation of motion, and takes the form

$$G_{\mu\nu} = 8\pi G_N \langle\psi| T_{\mu\nu} |\psi\rangle_{ren}, \tag{1.0.4}$$

where G_N is the Newton's constant, and we have inserted the renormalized value for the quantum matter field on the right hand side. This equation should, in general, be evaluated case by case. Note that in the 4D spherically symmetric case, we determine $a(r)$ and $A(r)$ in the metric (1.0.3) using (1.0.4), and thus the solution must satisfy (1.0.4). At the same time, we know that since the considered region (inside a Schwarzschild black hole) is expected to have high energy density, the matter field can be well-approximated by conformal field

doi:10.6342/NTU202302515

theories. Hence, we consider the 4 dimensional Weyl anomaly on the right hand side of Eq. (1.0.4), and it takes the form

$$\langle\psi|\, T^{\mu}_{\ \mu}\, |\psi\rangle_{ren} = \hbar(c_W\mathcal{F} - a_W\mathcal{G} + b_W\Box R), \tag{1.0.5}$$

where $\mathcal{F}$ is the square of Weyl tensor, $\mathcal{G}$ is the Gauss-Bonnet term, which are

$$\mathcal{F} \equiv C_{\alpha\beta\gamma\delta}C^{\alpha\beta\gamma\delta} = R_{\alpha\beta\gamma\delta}R^{\alpha\beta\gamma\delta} - 2R_{\alpha\beta}R^{\alpha\beta} + \frac{1}{3}R^2,$$
$$\mathcal{G} \equiv R_{\alpha\beta\gamma\delta}R^{\alpha\beta\gamma\delta} - 4R_{\alpha\beta}R^{\alpha\beta} + R^2.$$

a_W and c_W are dependent on the content of matter fields, see Sec. 3.2 for more details. b_W is a coefficient dependent of a_W and c_W, after regularization. In this thesis, we set $b_W = 0$ for simplicity. The discussion for generic b_W is considered in [15]. We then obtain a state-independent constraint, that is, the trace of semi-classical Einstein equation (1.0.4) with 4D Weyl anomaly (1.0.5). Still, since we have 2 functional degrees of freedom, $a(r)$ and $A(r)$ to fix, we are still one constraint short.

Therefore, we consider an equation of state in order to make this system solvable. Since we can regard the diagonal part of Einstein tensor as energy density, radial pressure, and tangential pressures (the tt, rr, and $\theta\theta/\phi\phi$ components, respectively), we assume their proportionality to set an equation of state. For simplicity, we consider an equation of state with one parameter, providing us three possibilities:

$$-G^{t}_{\ t} \propto G^{r}_{\ r}, \tag{1.0.6}$$
$$G^{r}_{\ r} \propto G^{\theta}_{\ \theta}, \tag{1.0.7}$$
$$-G^{t}_{\ t} \propto G^{\theta}_{\ \theta}. \tag{1.0.8}$$

doi:10.6342/NTU202302515

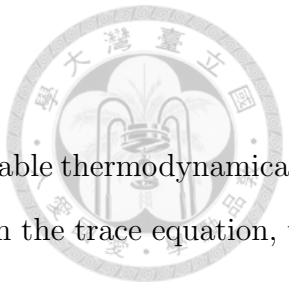

In chapter 4, we discuss all three cases, and find only one of them is stable thermodynamically to implement. After adopting a suitable equation of state along with the trace equation, we have a nonlinear differential equation for $a(r)$ to solve.

In chapter 5, we analyze how the solutions can be found using asymptotic series. From the analysis, we find a special type of solutions. It predicts a region of high energy density, cannot be obtained in perturbative (in $\hbar$) analysis, and is responsible to determine the value of r_{sur}.

The value of r_{sur} turns out to be larger than the size of horizon: $r_{sur} \approx a_0 + O({a_0}^{-1})$, where a_0 is the Schwarzschild radius of a black hole and the coefficient of $O(a^{-1})$ term is positive. It suggests a horizonless structure, but different from dark stars[1] in that the potentially large back-reactions are included in our analysis. As a matter of fact, in the region between Schwrzschild radius a and $r_{sur} > a$, the matter fields are highly excited, and the curvature at $r = a$ is infinite, suggesting a firewall paradigm.

All possible solutions with proper physical conditions are constructed in chapter 6. In there, we find that given ADM mass of a black hole, there exists variety of possible internal ($r \leq r_{sur}$) structures. Combining with the feature of horizonless, this suggests a similar situation with fuzzballs [16].

Due to the degenerate nature of the solutions found in previous chapter (several internal structures correspond to a single observable), we tried to calculate the entropy in chapter 6. Surprisingly, we recover the entropy area law.

After discovering all the possible static solutions, it is important to check whether these solutions are stable, that is, to check the time-evolution of these static solutions. However, it is almost impossible to check their full time-dependent behaviors. Hence, in chapter 7, we

[1]Dark stars are astronomical objects that has size slightly larger than its Schwarzschlid radius, evaporating, but the back-reaction of particle creation on geometry is ignored [16].

doi:10.6342/NTU202302515

are going to check their time-dependence in short time interval. That means first we assume

$$a(t,r) = a_{static}(r) + \epsilon_t b(t,r), \tag{1.0.9}$$

where $a_{static}(r)$ are the solutions obtained in previous chapters. Then, we solve the time-dependent equation up to $O(\epsilon_t)$. The $O(\epsilon_t)$ time dependence results we obtain suggest some instability, and thus equations with higher order in ϵ_t are important to understand, which will be done in future work.

Note that in chapter 2 we briefly mention about the history of quantum black holes.

doi:10.6342/NTU202302515

Chapter 2

Brief History of Quantum Black Holes

In 1973, Penrose and Hawking proposed their singularity theorems based on general relativity [17]. The theorem states that the collapse of objects, due to gravity, will not stop even after horizon forms, but shrink to a point to create a singularity. This implies 2 things: black hole exists and quantum aspects of black holes are essential. That is because nothing stops a collapse of matters, and eventually physics at short distance, that is, quantum theory, becomes important.

At the time, physicists were interested in formulating black hole mechanics in analogy to thermodynamics; for example, Benkenstein conjectured black holes have finite entropy proportional to its surface area A [18]. These works caught Hawking's attention. He then tried to understand the relationship between thermodynamics and geometries. His approach starts from formulating matters that build up a black hole as matter fields and consider quantum field theory under the influence of classical black holes. In mid-70s, he discussed in great details about this semi-classical system, and found that black holes can radiate, which is now known as the *Hawking radiation* [1, 13]. These radiation not only can have back-reactions to the background geometries, but it also makes black holes can have influence on

doi:10.6342/NTU202302515

regions outside horizon, resulting a way to properly define temperature of black holes. Based on the result, Hawking further went on to complete the formulation of black hole mechanics. In his calculation, he also showed the formula for entropy S to be $S = A/4$, which is known as *Bekenstein-Hawking entropy*.

Since then, physicists have been conducting extensive research on the quantum nature of black holes using various approaches, such as quantum field theory in curved spacetime and semi-classical gravity [19].

The first one deals with how fields can be quantized in curved background. Researchers discussed a variety of phenomenons with this setup. Casimir effects from boundaries and topology [20–26], and Hawking radiation of black holes [1,13,27–30] are some of the examples that were discussed.

The second one takes a step further and considers the back-reactions of the quantum effects on background geometries. In this case, since the background is not quantized, the back-reactions from quantum fields on background geometries should be evaluated as their expectation values. However, these expectation values can be divergent, meaning that regularizing them becomes important. Adiabatic [31–34], "n-wave" [35–37], and zeta function [38–41] regularizations are some of the well-developed schemes. Despite the existence of different schemes, Wald showed the eventual results is independent of regularization [42,43].

To sum up, in semi-classical gravity, solving semi-classical Einstein equation (1.0.4) is key to make the whole theory self-consistent. An interesting example is the KMY model [11]. They discuss from formation to evaporation of a black hole. Surprisingly, they find that throughout the process, neither horizons nor singularities appear, and the static solution exists, which implies thermodynamics still applies. That is an example to fix the problem we mentioned in the first paragraph of this chapter! Due to its robust correctness in field theoretics, it catches some eyes, and several follow-up works are done [6–10, 12, 44–46].

doi:10.6342/NTU202302515

Chapter 3

Equation of Motion and Constraints

In this chapter, we are going to write down our equation of motion, and physical constraints.

3.1 Equation of Motion

In this section, we are going to write down the equation of motion with 4 dimensional spherically symmetric static metric. The general form of the time-independent metric is as mentioned in Eq. (1.0.3), and for convenient we state it here again:

$$ds^2 = -e^{A(r)}\left(1-\frac{a(r)}{r}\right)dt^2 + \frac{1}{1-\frac{a(r)}{r}}dr^2 + r^2 d\Omega_2, \tag{3.1.1}$$

where $a(r)$ can be interpreted up to a proportional constant as mass, $M(r)$, enclosed in a sphere of raidus r centered at origin [47]:

$$M(r) = \frac{a(r)}{2G_N} = 4\pi\int_0^r dr r^2 \left\langle -T^t{}_t(r)\right\rangle . \tag{3.1.2}$$

doi:10.6342/NTU202302515

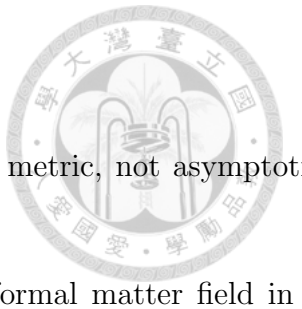

Note again that since we are connecting to external Schwarzschild metric, not asymptotic flat at infinity, we, in general, have $e^{A(r)}$ as an additional factor.

Next, we set up the semi-classical Einstein equation with conformal matter field in 4 dimension. Since the quantum effect is on the trace of energy momentum tensor, we pick up only the trace equation, which takes the form

$$\begin{aligned} G^{\mu}_{\ \mu} &= 8\pi G_N \langle\psi| T^{\mu}_{\ \mu} |\psi\rangle_{ren} \\ &= 8\pi G_N \hbar (c_W \mathcal{F} - a_W \mathcal{G}) \\ &\equiv \gamma \mathcal{F} - \alpha \mathcal{G} \end{aligned} \tag{3.1.3}$$

where $\mathcal{F}$ is the square of Weyl tensor, $\mathcal{G}$ is the Gauss-Bonnet term, which are

$$\begin{aligned} \mathcal{F} &\equiv C_{\alpha\beta\gamma\delta} C^{\alpha\beta\gamma\delta} = R_{\alpha\beta\gamma\delta} R^{\alpha\beta\gamma\delta} - 2R_{\alpha\beta} R^{\alpha\beta} + \frac{1}{3} R^2, \\ \mathcal{G} &\equiv R_{\alpha\beta\gamma\delta} R^{\alpha\beta\gamma\delta} - 4R_{\alpha\beta} R^{\alpha\beta} + R^2, \end{aligned}$$

and α and γ are defined as $(8\pi {l_P}^2 \hbar) a_W$ and $(8\pi {l_P}^2) c_W$[1], respectively. Note that Eq. (3.1.3) is independent of state $|\psi\rangle$, so we are not concentrating on any specific field configurations up to this point.

Here we have one constraint from the trace equation, but 2 functions, $a(r)$ and $A(r)$, to be solved. Hence, we are going to introduce an equation of state to complete the setup in chapter 4. In the chapter, we discuss suitable choice of equation of state, rather using the naive isotropic assumption. After adopting an additional constraint, we then can solve the whole setup without ambiguity.

[1] ${l_P}^2 = G_N \hbar$

doi:10.6342/NTU202302515

3.2 Constraints on Parameters

In this section, we are going to consider the physical constraints of the parameters in our system.

First, a_W and c_W depend on the content of matter fields. In free theory, they are

$$a_W = \frac{1}{5760\pi^2}(n_s + 11n_f + 62n_v),$$
$$c_W = \frac{1}{1920\pi^2}(n_s + 6n_f + 12n_v),$$

where n_s, n_f, and n_v are the number of scalar, fermion, and vector fields, respectively [2,48]. Their ratio is also bounded as

$$\frac{1}{3} \leq \frac{a_W}{c_W} = \frac{\alpha}{\gamma} \leq \frac{31}{18}, \tag{3.2.1}$$

where the left bound is obtained from by taking $n_s \to \infty$, and the right one comes from the limit $n_v \to \infty$. Interestingly, this bound is still valid even when interactions are introduced [49].

Second, since we consider only unitrary fields, a_W, c_W (or α, γ) are assumed to be positive.

To elaborate, we have

$$\alpha, \gamma > 0, \tag{3.2.2}$$

$$\alpha, \gamma \sim N\hbar G_N = N{l_P}^2, \tag{3.2.3}$$

$$\frac{1}{3} \leq \frac{a_W}{c_W} = \frac{\alpha}{\gamma} \leq \frac{31}{18}. \tag{3.2.4}$$

doi:10.6342/NTU202302515

3.3 Constraints on $a(r)$

Since our setup is designed to solve the region where $r \leq r_{sur}$ and connect to the external Schwarzschild metric at $r = r_{sur}$, $a(r)$ here is defined within $r \leq r_{sur}$ and must connect, at least, continuous at junction point $r = r_{sur}$. That is to ask $a(r_{sur}) = a_0$, where a_0 is the ADM mass of the black hole.

Speaking of the singularity of the system in terms of $a(r)$, the naive expectation will be that $a(r)$ itself is singular, which means that $a \to \pm\infty$. However, the system singularity can be checked with curvature invariants. Take scalar curvature for example, it has the form

$$R = \frac{2ra''(r) + a'(r)\left(3rA'(r) + 4\right) + \left(a(r) - 4r\right)A'(r) - r(r - a(r))\left(2A''(r) + A'(r)^2\right)}{2r^2}. \tag{3.3.1}$$

First of all, we have an expected singularity at $r = 0$, which is the same as with the Schwarzschild metric. The news here is the singularity also depends on $A'(r)$ and its derivative. As we will see in the next chapter, all three kinds of equations of state we considered have an expression $A'(r) \sim (r - a(r))^{-m}$ where m is some positive integer. This makes the curvature invariants go to $\pm\infty$, making another singularity, $a(r) = r$, of our system.

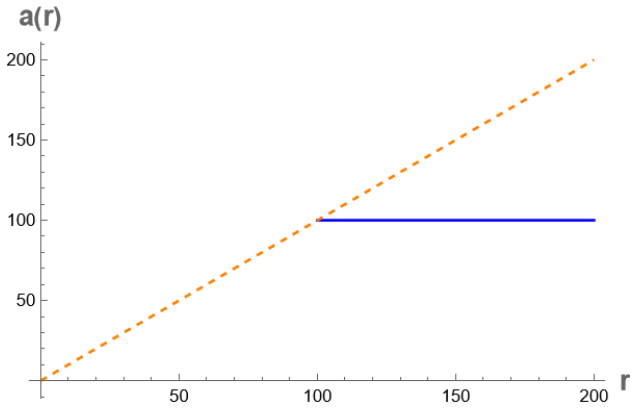

Figure 3.1: Graph to script

doi:10.6342/NTU202302515

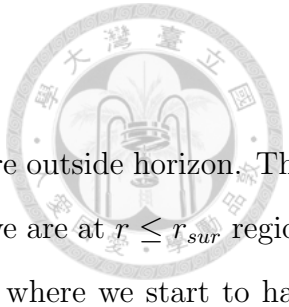

To sum up, when we are at $r \geq r_{sur}$, a_0 is less than r, since we are outside horizon. That will look something like the blue line in Fig. (3.1). However, when we are at $r \leq r_{sur}$ region, the value of $a(r)$ can never grow beyond $a = r$, which is the limit where we start to have event horizon. In fact, when $a(r)$, or naively just mass, grows to this limit, the curvature becomes singular, suggesting that our system is proposing a firewall paradigm. Also, since $a(r)$ represents cumulative mass from origin to r, its value is expected to be positive. Hence, the singularity of our system in terms of $a(r)$ should be $a = 0$ and $a = r$. That is, the allowed region is the triangle region in between the orange dotted line and $a = 0$ in Fig. (3.1).

doi:10.6342/NTU202302515

Chapter 4

Equation of State and Asymptotic Solutions

Up to now we have 2 unknown functions, $A(r)$ and $a(r)$, to solve but with only 1 constraint Eq. (3.1.3). A common treatment is to introduce an equation of state to drop the additional degrees of freedom. The physical observables we can use to introduce equation of state are the energy density and pressures. These are the components on the trace of Einstein tensor (through semi-classical Einstein tensor), that is, $-G_t{}^t$, $G_r{}^r$, and $G_\theta{}^\theta$ for energy density, radial pressure, and tangential pressure, respectively. By assuming a proportional relation among them, we can obtain a one-parameter equation of state, which are

$$G^r{}_r = w_1 G^\theta{}_\theta, \tag{4.0.1}$$

$$-G^t{}_t = w_2 G^\theta{}_\theta, \tag{4.0.2}$$

$$-G^t{}_t = w_3 G^r{}_r. \tag{4.0.3}$$

In the following sections, we are going to talk about the physical asymptotic solutions at

doi:10.6342/NTU202302515

large r for each case. That is to consider the ansatz

$$a(r) \in \text{span}\{r^k, r^{k-1}, r^{k-2}, \cdots : k \in \mathbb{R}\}, \tag{4.0.4}$$

where we assume r^k is the leading order of the series of solutions. Due to the above assumption of ansatz, we should first find the leading order k. That can be done through solving the equation of motion for $a(r)$ in each cases at leading order in large r limit. After finding the leading order individually, we then complete the asymptotic series.

Next we discuss the principle to select form of equation of state.

4.1 Eq. (4.0.1) and its Asymptotic Solutions

By combining Eq. (3.1.3) with the equation of state, Eq. (4.0.1), we obtain the equation of motion for $a(r)$. The general case is, however, lengthy and not informative, so we omit it here. We, in the following, only mention main results derived from this procedure.

First of all, from Eq. (4.0.1), we obtain an equation of $a(r)$, $A'(r)$, and $A''(r)$. That is,

$$A''(r) = \frac{Q_1(r)}{2rw_1(r - a(r))} \tag{4.1.1}$$

where

$$\begin{aligned} Q_1(r) =& 2rw_1 a''(r) + a'(r)\left(3rw_1 A'(r) - 4\right) \\ &+ A'(r)\left(rw_1(a(r) - r)A'(r) - (w_1 + 4)\, a(r) - 2r\,(w_1 - 2)\right). \end{aligned}$$

This shows $A''(r) \sim (r - a(r))^{-1}$. One can also check the form of $A'(r)$ explicitly with the setup, and find that $A'(r) \sim (r - a(r))^{-m}$ where m is some positive integer. Hence, the claim

doi:10.6342/NTU202302515

made in Sec. 3.3 about the singularity structure in $a(r)$ is true.

Next, we focus on the asymptotic solutions. With Eqs. (1.0.4) and (4.0.1), we can write down the differential equation that $a(r)$ must satisfy. Then, by inserting the ansatz (4.0.4) to the differential equation for $a(r)$ at $r \gg l_P$, we solve it at leading order (of r). From the differential equation, we select out all possible leading orders at large r. They are r^{4k}, r^{3k+3}, r^{2k+6}, and r^{k+7}, and we plot their powers with respect to k in Fig. 4.1 There are two

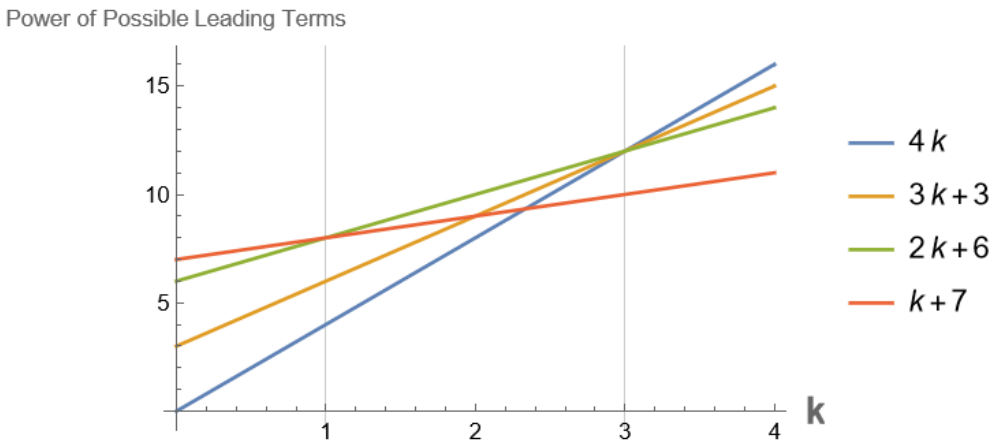

Figure 4.1: Plot for power of possible leading terms with respect to k with equation of state, Eq. (4.0.1)

ways for these leading terms (dependent on k) to vanish. One is to have the coefficient of a single leading term vanish, and the other one is to have multiple leading terms to cancel each other. From Fig. 4.1, we can see that single leading term to vanish, we will separate the cases into 3: $k < 1$, $1 < k < 3$, and $k > 3$. However, it can happen only when $k = 0$ or $k > 3$. Here we provide a sufficient proof: When $k < 1$, the leading power is r^{k+7} with coefficient $27k(k-3)$. It vanishes when $k = 0, 3$, where only $k = 0$ is in the range. When $1 < k < 3$, the leading power is r^{2k+6} with coefficient $-9k(k-15)$. It vanishes when $k = 0, 15$, where nothing is in the range. Therefore, single leading term cancellation can only happen when $k = 0$ and $k > 3$. Since $k > 3$ can only hit singularities (as mentioned in Sec. 3.3) quickly, we simply discard this case, leaving only $k = 0$. As for multiple leading terms cancellation,

doi:10.6342/NTU202302515

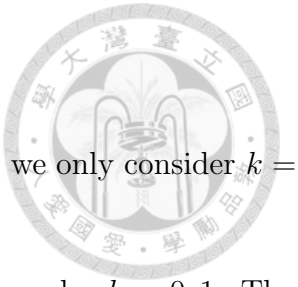

it can happen only when $k = 1, 3$, see Fig. 4.1. For the same reason, we only consider $k = 1$ case.

Next, we can find the asymptotic solutions starting from leading order $k = 0, 1$. These series are

$$a_{0,(3.0.1)}(r) = c_0 + \frac{4c_0^2(\gamma-\alpha)}{r^3} - \frac{3c_0^3\,(w_1+2)\,(\alpha-\gamma)}{r^4\,(10w_1+4)} + O(r^{-5}), \tag{4.1.2}$$

$$\begin{aligned} a_{1,(3.0.1)}(r) =& \frac{(w_1+2)}{w_1\,(w_1+3)+3} r \\ & - \frac{4\,(w_1+1)\,(w_1^2+w_1+1)\,(2\alpha w_1\,(w_1+2) - 3\gamma\,(w_1+1)^{\,2})}{(w_1\,(w_1+3)+3)^{\,2}\,(w_1\,(w_1\,(w_1+2)+3)+3)\,r} + O(r^{-3}), \end{aligned} \tag{4.1.3}$$

where c_0 is some real constant to be fixed.

4.2 Eq. (4.0.2) and its Asymptotic Solutions

In this section, we are going to proceed with the same procedure as in Sec. 4.1.

First, we verify the claim in Sec. 3.3. The form of $A''(r)$ is

$$A''(r) = \frac{Q_2(r)}{2rw_2(r-a(r))} \tag{4.2.1}$$

where

$$Q_2(r) = 2rw_2a''(r) + a'(r)\,(3rw_2A'(r)+4) - w_2A'(r)\,(r(r-a(r))A'(r) + a(r) + 2r)\,.$$

Again, $A''(r) \sim (r-a(r))^{-1}$, and one can check that $A'(r) \sim (r-a(r))^{-m}$ where m is positive integer. That proves the statement in Sec. 3.3.

Next, we focus on the asymptotic solutions with Eq. (4.0.2). In this case, we obtain the

doi:10.6342/NTU202302515

equation of motion for $a(r)$ by inserting Eq. (4.0.2) into Eq. (3.1.3). By assuming Eq. (4.0.4), we obtain all possible the leading order of equation of motion for $a(r)$. They are r^{k+19}, r^{2k+18}, r^{3k+15}, r^{4k+12}, r^{5k+9}, and r^{6k+6}, and we plot their power with respect to k in Fig. 4.2.

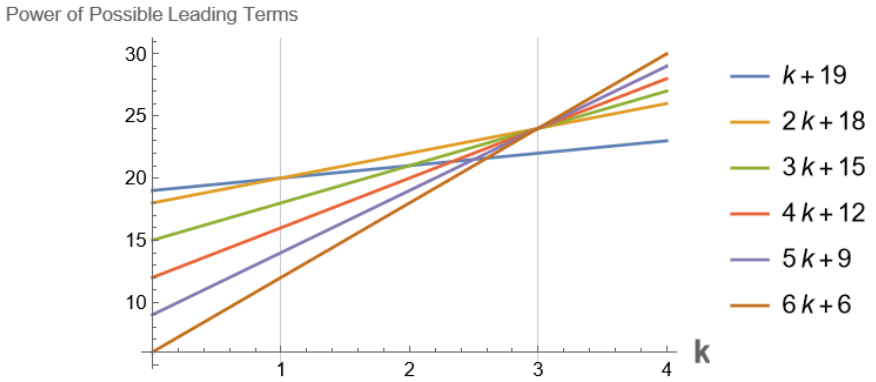

Figure 4.2: Plot for power of possible leading terms with respect to k with equation of state, Eq. (4.0.2)

For single leading term cancellation, we again split the case into 3: $k < 1$, $1 < k < 3$, and $k > 3$. We again only focus on the two cases where $k < 3$, since $k > 3$ is singular. When $k < 1$, we have r^{k+19} to be the leading term with coefficient proportional to $k\,(w - k\,(w-2))$. This vanishes when $k = 0, \frac{w}{w-2}$, which clearly captures $k = 0$. For $k = \frac{w}{w-2}$ within $k < 1$, we can fix the range as $w < 2$. At the same time, since w should be positive[1], we can fix the range of w as $0 \leq w \leq 2$. With this range of w, the value of k is negative. Since energy density is proportional to $a'(r)$, the asymptotic solution of this kind must describe negative energy density, creating instability, and therefore, we discard this case. When $1 < k < 3$, we have the leading term with coefficient to be proportional to $k\,(k\,(w-2) + w - 2w^2)\,r^{2k+18}$. Then its coefficient vanishes at $k = 0, \left(2 + \frac{3}{w-2}\right) w$. $k = 0$ does not fit in this case, and one can check neither does $k = \left(2 + \frac{3}{w-2}\right) w$. Hence, up to now we only have candidate $k = 0$.

After the single leading term case, we can read of from Fig. 4.2 that the cancellation

[1]Otherwise, between energy density and tangential pressure, there must be one to be negative, creating instability to the system.

doi:10.6342/NTU202302515

among multiple leading terms happens at $k = 1, 3$. Again, since $k = 3$ is singular, we keep only $k = 1$, making the physical candidates $k = 0, 1$ only, just like in Sec. 4.1.

$$a_{0,(3.0.2)}(r) = c_0 + \frac{8a_0^2 w_2(\gamma-\alpha)}{r^3(2w_2-3)} - \frac{3a_0^3 w_2(2w_2-1)(\alpha-\gamma)}{2r^4(2w_2-3)(5w_2-8)} + O(r^{-5}), \tag{4.2.2}$$

$$a_{1,(3.0.2)}(r) = \frac{w}{w^2-w+1}r + \frac{4(w-2)(w-1)w\left(3\gamma(w-1)^2-2\alpha(w-2)w\right)}{((w-1)w+1)^2(w((w-4)w+7)-3)r} + O(r^{-3}), \tag{4.2.3}$$

where, again, c_0 is some real parameter to be fixed.

4.3 Eq. (4.0.3) and its Asymptotic Solutions

In this section, we proceed with equation of state Eq. (4.0.3) and the same procedure as in Sec. 4.1.

We first prove the claim stated in Sec. 3.3. $A'(r)$ takes the form

$$A'(r) = \frac{2a'(r)}{\eta(r-a(r))}. \tag{4.3.1}$$

In this case, we have $A'(r) \sim (r-a(r))^{-1}$, implying $A''(r) \sim (r-a(r))^{-2}$. Since all three cases have $(r-a(r))$ in the denominator of $A'(r)$ and $A''(r)$, the singular structure of our system in terms of $a(r)$ is as claimed in Sec. 3.3.

The asymptotic solutions can also be obtained from the same procedure. By inserting Eq. (4.0.3) to Eq. (3.1.3) with ansatz Eq. (4.0.4), we have the possible leading order terms: r^{k+5}, r^{2k+4}, r^{3k+3}, and r^{4k}, and their powers are plotted with respect to k in Fig. 4.3.

Then, we again consider conditions when single and multiple leading terms vanishes.

doi:10.6342/NTU202302515

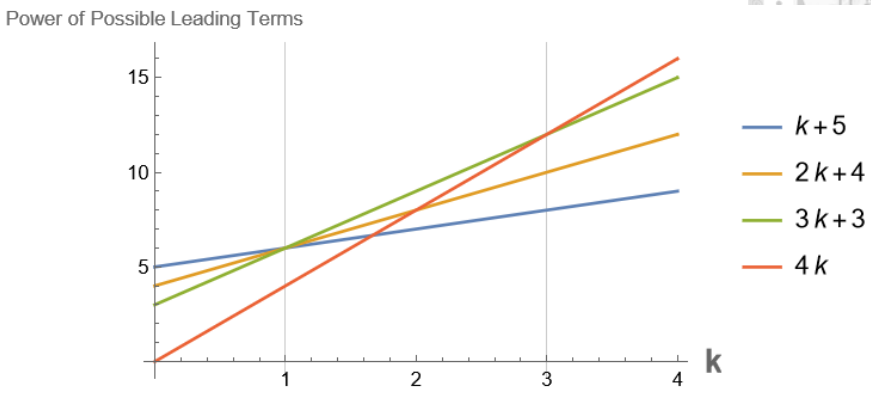

Figure 4.3: Plot for power of possible leading terms with respect to k with equation of state, Eq. (4.0.3)

Starting with single leading term, we have three possible domains of k: $k < 1$, $1 < k < 3$, and $k > 3$. We will only focus on the first two as the third one is identified as singular.

When $k < 1$, the leading term is r^{k+5} with coefficient proportional to $k(k - w_3)$. The coefficient vanishes when $k = 0, w_3$. Here we pick up $k = 0$. For $k = w_3 < 1$, as we will see in the next subsection, it predicts a velocity field of the corresponding matter field exceed the speed of light, so we do not consider it in the following discussion. When $1 < k < 3$, the leading term is r^{3k+3} with coefficient proportional to $k(k - \frac{w_3(1+3w_3)}{w_3-1})$, which vanishes at $k = 0, \frac{w_3(1+3w_3)}{w_3-1}$. One can check that neither do these two possibility have values in $1 < k < 3$. Hence, we only pick up $k = 0$ from single leading term cancellation. When $k = 1, 3$, we can have cancellation among multiple leading terms. Since $k = 3$ is singular, we, overall, only focus on $k = 0, 1$.

doi:10.6342/NTU202302515

The corresponding asymptotic solutions are

$$a_{0,(3.0.3)}(r) = c_0 + \frac{2c_0^2\eta(\gamma-\alpha)}{(3-\eta)r^3} + \frac{3c_0^3\eta(\gamma-\alpha)}{2(8-3\eta)(3-\eta)r^4} + O(r^{-5}), \tag{4.3.2}$$

$$a^{(slope=1)}_{1,(3.0.3)}(r) = r - \frac{2\gamma}{3\eta^2 r} + \frac{4\gamma\left(\gamma(\eta(\eta+6)-2)-6\alpha\eta^2\right)}{9\eta^4 r^3} + O(r^{-5}), \tag{4.3.3}$$

$$a^{(slope\neq 1)}_{1,(3.0.3)}(r) = \frac{(\eta-1)\eta}{(\eta-1)\eta+1}r + \frac{2(\eta-1)^2\eta(3\gamma-2\alpha(2-\eta)\eta)}{((\eta-1)\eta+1)^2(3-(2-\eta)\eta(\eta+1))r} + O(r^{-3}), \tag{4.3.4}$$

where c_0 is some real parameter to be fixed, and we switch the proportional constant from w_3 to η such that $w_3 = \frac{\eta}{2-\eta}$ (or $\eta = \frac{2w_3}{w_3+1}$), that is

$$-G^t{}_t = \frac{\eta}{2-\eta}G^r{}_r, \tag{4.3.5}$$

and we will use this convention through the paper.

4.4 Why Eq. (4.0.3)

Since our setup is to patch the region $r \leq r_{sur} \sim a_0$ where a_0 is the Schwarzschild radius in $r > r_{sur}$ region, we expect $a(r_{sur}) = a_0$ so that we can connect to external Schwarzschild metric. Since we have identify all the asymptotic solutions in Secs. 4.1– 4.3, and find the only possible type is those with $a(r) \approx r$. Note that asymptotic solutions with $a(r) \approx c_0$ are as well options to connect at junction, but they will soon hit $a = r$ singularity; therefore, we do not consider this type as a possibility here. Therefore, we have to test whether asymptotic solutions, $a(r) \approx r$, in all three case are physical, which means their energy density and pressures must be positive. In the following, we calculate the diagonal components of Einstein tensor in each cases, and we will see only the case with Eq. (4.0.3) is physical.

With Eq. (4.0.1), the asymptotic solution with $a(r) \approx r$ is described by Eq. (4.1.3) with

doi:10.6342/NTU202302515

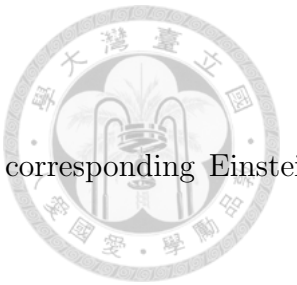

$w_1 = -1$. The form of $a(r)$ and the diagonal components of the corresponding Einstein tensor are

$$a(r) = r - \frac{16\alpha^2}{r^3} - \frac{512\alpha^3}{r^5} + O(r^{-7}), \tag{4.4.1}$$

$$-G^t{}_t = \frac{1}{r^2} + \frac{48\alpha^2}{r^6} + \frac{2560\alpha^3}{r^8} + O(r^{-10}), \tag{4.4.2}$$

$$G^r{}_r = -\frac{1}{r^2} - \frac{8\alpha}{r^4} - \frac{144\alpha^2}{r^6} - \frac{128\alpha^2(105\alpha + 8\gamma)}{3r^8} + O(r^{-10}), \tag{4.4.3}$$

$$G^\theta{}_\theta = \frac{1}{r^2} + \frac{8\alpha}{r^4} + \frac{144\alpha^2}{r^6} + \frac{128\alpha^2(105\alpha + 8\gamma)}{3r^8} + O(r^{-10}). \tag{4.4.4}$$

From the expression, we can find two things. First, at junction position $r = r_{sur}$, we have

$$a_0 = a(r_{sur}) = r_{sur} - \frac{16\alpha^2}{{r_{sur}}^3} + \dots. \tag{4.4.5}$$

We, therefore, can find the size of the inner region as

$$r_{sur} \approx a_0 + \frac{16\alpha^2}{{a_0}^3}, \tag{4.4.6}$$

suggesting $r_{sur} > a_0$. Second, the radial pressure, $G^r{}_r$, is negative, so we should discard this case.

With Eq. (4.0.2), the asymptotic solution with $a(r) \approx r$ is described by Eq. (4.2.3) with $w_2 = 1$. The form of $a(r)$ and the diagonal components of the corresponding Einstein tensor

doi:10.6342/NTU202302515

are

$$a(r) = r - \frac{16\alpha^2}{r^3} + \frac{384\alpha^3}{r^5} + O(r^{-7}), \tag{4.4.7}$$

$$-G^t{}_t = \frac{1}{r^2} + \frac{48\alpha^2}{r^6} - \frac{1920\alpha^3}{r^8} + O(r^{-10}), \tag{4.4.8}$$

$$G^r{}_r = -\frac{1}{r^2} + \frac{8\alpha}{r^4} - \frac{80\alpha^2}{r^6} + \frac{256\alpha^2(33\alpha+\gamma)}{3r^8} + O(r^{-10}), \tag{4.4.9}$$

$$G^\theta{}_\theta = \frac{1}{r^2} + \frac{48\alpha^2}{r^6} - \frac{1920\alpha^3}{r^8} + O(r^{-10}), \tag{4.4.10}$$

which is very similar to the case with Eq. (4.0.1), and the difference comes in from $O(r^{-5})$ in $a(r)$. Again, from the same argument as above,

$$r_{sur} \approx a_0 + \frac{16\alpha^2}{{a_0}^3} > a_0, \tag{4.4.11}$$

and since its radial pressure is negative, we discard this case.

However, with Eq. (4.0.3), the asymptotic solution with $a(r) \approx r$ is described by Eq. (4.3.3). The form of $a(r)$ and the diagonal components of its Einstein tensor are

$$a(r) = r - \frac{2\gamma}{3\eta^2 r} + \frac{4\gamma\left(\gamma(\eta(\eta+6)-2) - 6\alpha\eta^2\right)}{9\eta^4 r^3} + O(r^{-5}), \tag{4.4.12}$$

$$-G^t{}_t = \frac{1}{r^2} + O(r^{-4}),\ G^r{}_r = \frac{2-\eta}{\eta}\frac{1}{r^2} + O(r^{-4}),\ G^\theta{}_\theta = \frac{3}{2\gamma} + O(r^{-2}). \tag{4.4.13}$$

In this case,

$$r_{sur} \approx a_0 + \frac{2\gamma}{3\eta^2 a_0}, \tag{4.4.14}$$

and all physical quantities are positive.

doi:10.6342/NTU202302515

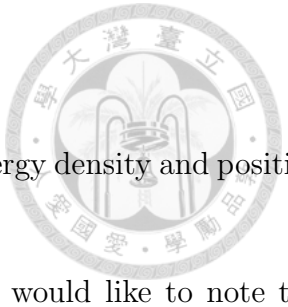

Overall, from elimination due to physical constraints (positive energy density and positive pressure), we are left with only one option: Eq. (4.0.3).

After we see Eq. (4.0.3) is the equation of state to choose, we would like to note the problem remaining from previous subsection. That is, when $k < 1$, single leading term cancellation can happen when $k = w_3 < 1$. It seems fine, until we consider consistency on Eq. (4.4.12) inside metric. After these inputs are inserted, we can check the causality condition of the matter fields. That means that the speed of these matter fields at classical level cannot exceed the speed of light in local Lorentz frame. The speed takes the form

$$\left|\frac{dl}{d\tau}\right| = 2 - \eta, \tag{4.4.15}$$

which implies that a physical theory can only have η in between 1 and 2. After we translate this range into w_3, it demands $w_3 > 1$, and that is a contraction. Hence we do not have new physical asymptotic solutions in that case.

4.5 The $a(r)$-Equation

After using Eq. (4.0.3), we can eliminate one functional degree of freedom ($A(r)$) in the equation of motion Eq. (3.1.3). This becomes an equation of motion for $a(r)$ and we call it *the $a(r)$-equation*. It takes the form

$$-\frac{\gamma(2-\eta)}{3\eta(r-a(r))}a''(r)^2 + \mathcal{C}_1(r)a''(r) + \mathcal{C}_2(r) = 0, \tag{4.5.1}$$

doi:10.6342/NTU202302515

where

$$\begin{aligned}
\mathcal{C}_1(r) =& \frac{Q_1(r)}{3(\eta-2)\eta^2(r-a(r))^2r^2},\\
\mathcal{C}_2(r) =& \frac{\gamma(\eta-2)}{3\eta^3(r-a(r))^3}a'(r)^4 + \frac{Q_2(r)}{3(2-\eta)\eta^2(r-a(r))^3r}a'(r)^3\\
&+ \frac{Q_3(r)}{3(2-\eta)\eta(r-a(r))^3r^2}a'(r)^2 - \frac{Q_4(r)}{(2-\eta)(r-a(r))^3r^3}a'(r)\\
&+ \frac{12\eta(\alpha-\gamma)}{(2-\eta)r^4(r-a(r))}a(r)^2,
\end{aligned}$$

and

$$\begin{aligned}
Q_1(r) =& (\eta-2)r^2a'(r)^2(2\gamma(\eta-2)) + \eta ra'(r)(2\gamma(\eta-2)(4\eta-5)a(r) - 8\gamma(\eta-2)(\eta-1)r)\\
&+ 3\eta^2ra(r)\left(-4\alpha(\eta-2) + 4\gamma(\eta-2) - \left((\eta-2)r^2\right)\right)\\
&+ 3\eta^2a(r)^2(4\alpha(\eta-2) - 4\gamma(\eta-2))\\
&+ 3\eta^2r^2(\eta-2)r^2,
\end{aligned}$$

$$Q_2(r) = 8r\gamma(\eta-2)(\eta-1) - 2(\eta-2)a(r)\gamma(4\eta-5),$$

$$\begin{aligned}
Q_3(r) =& ra(r)\Big(2\eta(6\alpha(5-2\eta) + 2\gamma(8\eta-21)) - 24\alpha + 64\gamma + 3(\eta-2)r^2\Big)\\
&+ a(r)^2(12\alpha(\eta-2)(\eta-1) + \gamma(4(13-4\eta)\eta - 49))\\
&+ r^2\left(6\eta(2\alpha(\eta-2)) - 16\gamma(\eta-1)^2 - 3(\eta-2)r^2\right),
\end{aligned}$$

doi:10.6342/NTU202302515

$$
\begin{aligned}
Q_4(r) =& a(r)\Big(ra(r)\left(4\eta(-8\alpha+8\gamma)+36\alpha-36\gamma+(2\eta-1)r^2\right)\\
&+4a(r)^2(\alpha(4\eta-5)-4\eta\gamma+5\gamma)+(3-4\eta)r^4\\
&+2r^2(8\alpha(\eta-1)-8\eta\gamma+8\gamma)\Big)+2(\eta-1)r^5.
\end{aligned}
$$

This is a singular equation, since the power of highest order derivative term is not 1. To make it non-singular, we solve for $a''(r)$ algebraically, and find 2 branches of equations:

$$
a''(r)-\frac{1}{2\gamma(2-\eta)\eta r^2(r-a(r))}\left(\mathcal{F}_1(r)\pm\eta^{3/2}\left(r-a(r)\right)\sqrt{\mathcal{F}_2(r)}\right)=0 \tag{4.5.2}
$$

with

$$
\begin{aligned}
\mathcal{F}_1(r) =& -2\gamma\left(2-\eta\right)r^2a'(r)^2\\
&-2\gamma\eta r\left(\left(5-4\eta\right)a(r)+4\left(\eta-1\right)r\right)a'(r)\\
&+3\eta^2\left(r-a(r)\right)\left(4\left(\gamma-\alpha\right)a(r)+r^3\right) \qquad (4.5.3)\\
\mathcal{F}_2(r) =& -72\gamma\left(\eta-1\right)r^4a'(r)\\
&-48\alpha\gamma\left(2-\eta\right)r^2a'(r)^2\\
&+9\eta\left(8\left(\alpha-\gamma\right)a(r)\left(2\alpha a(r)-r^3\right)+r^6\right), \qquad (4.5.4)
\end{aligned}
$$

where we, for simplicity, call the $+/-$ one $+/-$ branch equation.

In chapter 5, we are going to analyze these equations in details and extract physical picture of black holes in chapter 6.

doi:10.6342/NTU202302515

4.6 Brief Discussion on Equation of State and Slope-1 Asymptotic Solution

So far, we have been assuming conformal symmetry and equation of state, and here we are going to discuss what we have found.

First of all, the usage of equation of state implicitly assumes the mean free path of the particle in the region is small. That means, in principle, we can only apply it to regions with high energy density.

Meanwhile, we have considered 3 different kinds of equations of state in our setup, and all of them seems to suggest 2 types of asymptotic behaviors. They are Schwarzschild-like ($O(r^0)$) and linear one ($O(r)$).

As we have calculated the energy density ($\sim -G^t{}_t$), we can argue the latter is totally fine. The problem is the former. It has low energy density, but always appears. A possible implication is that in regions with low energy densities, Schwarzschild metric can be used for approximation. Hence, in principle, we shall use Schwarzschild metric to represent those low energy density regions; however, since we know our Schwarzschild-like solution are the same as that of Schwarzschild at leading order, we still use the solution we got, and in chapter 5, we justify this movement numerically.

Note that this can be researched in more details. After finding the correct equation of state, or other constraint, one can fix this part of the model.

Second, regarding the linear asymptotic solutions with slope 1 (see Sec. 4.4), they are all non-perturbative results. That means the metric is singular at $\hbar \to 0$ limit, since their g_{rr}

doi:10.6342/NTU202302515

components take the form

$$g_{rr} = \frac{1}{1 - \frac{a(r)}{r}} \approx \frac{1}{-\hbar r^{-k}}, \tag{4.6.1}$$

where $k = 1$ for equation of state (4.0.3), $k = 3$ for equations of state (4.0.1) and (4.0.2), and $\hbar$ comes from α and γ. Also, independent of equations of state, they all predict r_{sur} to be larger than a_0, where a_0 is the ADM mass of the black hole. Even though only one of them has all positive energy density and pressures, they all predict horizonless "black holes". That means there are extra structure around horizon, in contrast to the classical description. In other words, black holes are NOT just empty holes.

doi:10.6342/NTU202302515

Chapter 5

Structure of Solution Space of the $a(r)$-Equation

We have established the reasoning of our setup including the usage of equation of state. In this chapter, we are going to focus on solving the $a(r)$-equation Eq. (4.5.1) asymptotically.

In Sec. 5.1, for completeness, we write the asymptotic solutions again with one additional case not mentioned above. Even though it is nonphysical due to its large negative energy density, it shows an example of why we did not discuss singular solutions in chapter 4.

Beyond the asymptotic solutions discovered in chapter 4, we as well analyze the linearized equation around each asymptotic solution in Sec. 5.2. That is, with assumption:

$$a(r) = a_{asymp}(r)(1 + \epsilon\mathcal{D}(r)),$$

we solve the equation up to $O(\epsilon)$ for $\mathcal{D}(r)$ given an $a_{asymp}(r)$. The solution $\mathcal{D}(r)$ tells us how the difference between true solution $a(r)$ and asymptotic solution $a_{asymp}(r)$ varies as r increases. When the difference is small, $\mathcal{D}(r)$ provides qualitative information. However,

doi:10.6342/NTU202302515

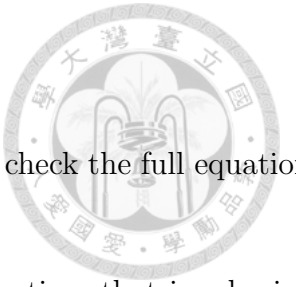

the difference may be large, and thus for completeness and rigor, we check the full equation, including all orders of ϵ, numerically in Sec. 5.3.

Throughout the procedure, we can extract all the desired information, that is, physical solutions allowed by both branches in Eq. (4.5.2).

5.1 Asymptotic Solutions

With the same procedure mentioned in Sec. 4.3, we can find three physical asymptotic solutions and one nonphysical one, where the nonphysical one was not mentioned previously. Note that we discuss the physical asymptotic solutions in Sec. 5.1.1.

Physical Asymptotic Solutions

The physical ones are the same as those in Sec. 4.3. For convenience, we summarize them here again each with one additional higher order term and a new name. Also, the corresponding leading behaviors of metrics, Einstein tensor, and Curvature invariants are summarized.

Low Density Asymptotic Solution: $a_S(r)$

Here we summarize quantities regarding low density asymptotic solution below. The form of $a(r)$ is

$$a_S(r) = c_0 + \frac{2c_0^2\eta(\gamma-\alpha)}{(3-\eta)r^3} + \frac{3c_0^3\eta(\gamma-\alpha)}{2(8-3\eta)(3-\eta)r^4} + O(r^{-5}), \tag{5.1.1}$$

doi:10.6342/NTU202302515

where c_0 is a free parameter to be fixed. The leading behavior ($r \gg l_P$) of metric is

$$\begin{aligned} ds^2 \approx &- \left(1 - \frac{c_0}{r} + \frac{2\eta(\alpha-\gamma){c_0}^2}{(3-\eta)r^4}\right) e^{-\frac{3\eta(\alpha-\gamma){c_0}^2}{(3-\eta)r^4}} dt^2 \\ &+ \left(1 - \frac{c_0}{r} + \frac{2\eta(\alpha-\gamma){c_0}^2}{(3-\eta)r^4}\right)^{-1} dr^2 + r^2 d\Omega^2, \end{aligned} \tag{5.1.2}$$

where $e^{A(r)}$ is determined by Eq. (4.3.1), and the corresponding energy density, pressures, and curvature invariants

$$\begin{aligned} -G^t{}_t =& \frac{6\eta(\alpha-\gamma){c_0}^2}{(3-\eta)r^6}, \\ G^r{}_r =& \frac{6(2-\eta)(\alpha-\gamma){c_0}^2}{(3-\eta)r^6}, \\ G^\theta{}_\theta =& -\frac{12(2-\eta)(\alpha-\gamma){c_0}^2}{(3-\eta)r^6}, \end{aligned} \tag{5.1.3}$$

and

$$\begin{aligned} R =& \frac{12(\alpha-\gamma)c_0^2}{r^6} + O(r^{-8}), \\ R_{\mu\nu}R^{\mu\nu} =& \frac{72\left(5\eta^2 - 18\eta + 18\right)(\alpha-\gamma)^2 c_0^4}{(3-\eta)^2 r^{12}} + O(r^{-13}), \\ R_{\mu\nu\alpha\beta}R^{\mu\nu\alpha\beta} =& \frac{12{c_0}^2}{r^6} + \frac{48(6-5\eta)(\alpha-\gamma)c_0^3}{(3-\eta)r^9} + O(r^{-10}). \end{aligned} \tag{5.1.4}$$

Medium Density Asymptotic Solutions: $a_\eta(r)$

Here we summarize quantities regarding moderate density asymptotic solution below. The form of $a(r)$ is

$$a_\eta(r) = \frac{(\eta-1)\eta}{(\eta-1)\eta+1} r + \frac{2(\eta-1)^2\eta(3\gamma - 2\alpha(2-\eta)\eta)}{((\eta-1)\eta+1)^2(3-(2-\eta)\eta(\eta+1))r} + O(r^{-3}). \tag{5.1.5}$$

doi:10.6342/NTU202302515

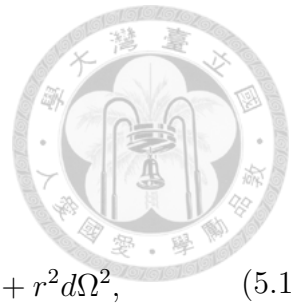

The leading behavior ($r \gg l_P$) of metric is

$$ds^2 \approx -\frac{1}{\eta^2-\eta+1}\left(\frac{r}{r_0}\right)^{2(\eta-1)} dt^2 + (\eta^2-\eta+1)dr^2 + r^2 d\Omega^2, \tag{5.1.6}$$

with corresponding energy density, pressures, and curvature invariants

$$\begin{aligned} -G^t{}_t &= \frac{(\eta-1)\eta}{(\eta^2-\eta+1)\,r^2}, \\ G^r{}_r &= -\frac{(2-\eta)(\eta-1)}{(\eta^2-\eta+1)\,r^2}, \\ G^\theta{}_\theta &= \frac{(\eta-1)^2}{(\eta^2-\eta+1)\,r^2}, \end{aligned} \tag{5.1.7}$$

and

$$\begin{aligned} &+O(r^{-4}), \\ R_{\mu\nu}R^{\mu\nu} &= \frac{2(\eta-1)^2\,(2\eta^2-4\eta+3)}{(\eta^2-\eta+1)^2\,r^4} + O(r^{-6}), \\ R_{\mu\nu\alpha\beta}R^{\mu\nu\alpha\beta} &= \frac{8(\eta-1)^2\,(\eta^2-2\eta+3)}{(\eta^2-\eta+1)^2\,r^4} + O(r^{-6}). \end{aligned} \tag{5.1.8}$$

High Density Asymptotic Solutions: $a_{den}(r)$

Here we summarize quantities regarding high density asymptotic solution below. The form of $a(r)$ is

$$a_{den}(r) = r - \frac{2\gamma}{3\eta^2 r} + \frac{4\gamma\,(\gamma(\eta(\eta+6)-2)-6\alpha\eta^2)}{9\eta^4 r^3} + O(r^{-5}). \tag{5.1.9}$$

The leading behavior ($r \gg l_P$) of metric is

$$ds^2 \approx -\frac{2\gamma}{3\eta^2 r^2} e^{\frac{3\eta r^2}{2\gamma}} dt^2 + \frac{3\eta^2 r^2}{2\gamma} dr^2 + r^2 d\Omega^2, \tag{5.1.10}$$

doi:10.6342/NTU202302515

with corresponding energy density, pressures, and curvature invariants

$$\begin{aligned} -G^t{}_t &= \frac{1}{r^2} + O(r^{-4}), \\ G^r{}_r &= \frac{2-\eta}{\eta}\frac{1}{r^2} + O(r^{-4}), \\ G^\theta{}_\theta &= \frac{3}{2\gamma} + O(r^{-2}), \end{aligned} \tag{5.1.11}$$

and

$$\begin{aligned} R &= -\frac{3}{\gamma} + O(r^{-2}), \\ R_{\mu\nu}R^{\mu\nu} &= \frac{9}{2\gamma^2} + O(r^{-2}), \\ R_{\mu\nu\alpha\beta}R^{\mu\nu\alpha\beta} &= \frac{9}{\gamma^2} + O(r^{-2}). \end{aligned} \tag{5.1.12}$$

Nonphysical but Interesting Asymptotic Solution

Negative Energy Density Asymptotic Solution $a_{neg}(r)$

This asymptotic solution is not mentioned in Sec. 4.3, since it is nonphysical and do not affect the argument in fixing equation of state. Here, we take it as an example of singular behaviors, and discuss in Sec. 5.1.1 why we do not include them in our physical solutions. This series stems from the other case of multiple leading term cancellation, which has leading order r^3, see Sec. 4.3.

Here we summarize its details below. The form of $a(r)$ is

$$a_{neg}(r) = \frac{\eta^2\left(2\eta^2-4\eta+3\right)r^3}{2(\eta-3)\left(2\alpha(\eta-1)\eta^2-\gamma(\eta-3)\right)} + \frac{p_n(r)}{p_d(r)} + O(r^{-1}), \tag{5.1.13}$$

doi:10.6342/NTU202302515

where

$$\begin{aligned} p_n(r) =& 3r\left(2\alpha\eta^4+\gamma\left(4\eta^3-19\eta^2+24\eta-9\right)\right) \\ p_d(r) =& \eta(2\alpha\eta\left(\eta^3-8\eta^2+15\eta-9\right))+\gamma\left(4\eta^4+9\eta^3-40\eta^2+42\eta-9\right). \end{aligned}$$

The leading behavior ($r \gg l_P$) of metric is

$$ds^2 \approx -\left(1-Kr^2\right)\left(\frac{r_0}{r}\right)^{\frac{6}{\eta}}dt^2+\left(1-Kr^2\right)^{-1}dr^2+r^2d\Omega^2, \tag{5.1.14}$$

where

$$K \equiv \frac{\eta^2(2(2-\eta)\eta-3)}{2(3-\eta)\left(2\alpha(\eta-1)\eta^2+\gamma(3-\eta)\right)}, \tag{5.1.15}$$

with corresponding energy density, pressures, and curvature invariants

$$\begin{aligned} -G^t{}_t =& -\frac{3\eta^2\left(2\eta^2-4\eta+3\right)}{2(3-\eta)\left(2\alpha(\eta-1)\eta^2+\gamma(3-\eta)\right)}+O(r^{-2}), \\ G^r{}_r =& -\frac{3\eta(2-\eta)\left(2\eta^2-4\eta+3\right)}{2(3-\eta)\left(2\alpha(\eta-1)\eta^2+\gamma(3-\eta)\right)}+O(r^{-2}), \\ G^\theta{}_\theta =& \frac{3\left(\left(\eta^2-3\eta+3\right)\left(2\eta^2-4\eta+3\right)\right)}{2\left(\left(3-\eta\right)\left(2\alpha(\eta-1)\eta^2+\gamma(3-\eta)\right)\right)}+O(r^{-2}), \end{aligned} \tag{5.1.16}$$

and

$$\begin{aligned} R =& -\frac{3\left(2\eta^2-4\eta+3\right)^2}{(3-\eta)\left(2\alpha(\eta-1)\eta^2+\gamma(3-\eta)\right)}+O(r^{-2}), \\ R_{\mu\nu}R^{\mu\nu} =& \frac{9\left(\eta^2-2\eta+3\right)\left(2\eta^2-4\eta+3\right)^3}{2(3-\eta)^2\left(\gamma(3-\eta)+2\alpha(\eta-1)\eta^2\right)^2}+O(r^{-2}), \\ R_{\mu\nu\alpha\beta}R^{\mu\nu\alpha\beta} =& \frac{3\left(2\eta^2-4\eta+3\right)^2\left(2\eta^4-8\eta^3+24\eta^2-36\eta+27\right)}{(3-\eta)^2\left(\gamma(3-\eta)+2\alpha(\eta-1)\eta^2\right)^2}+O(r^{-2}). \end{aligned} \tag{5.1.17}$$

doi:10.6342/NTU202302515

5.1.1 Brief Discussion on the Asymptotic Solutions

Before proceeding to the next section, we first understand these asymptotic solutions better with a brief discussion here.

Regarding physical cases, we can classify them in terms of their curvature invariants, which are proportional to energy density. From the highest one to the lowest one, we have $a_{den}(r)$, $a_\eta(r)$, and then $a_S(r)$, so they have their names. Among them, the $a_{den}(r)$ asymptotic solution is the most interesting, since its curvature is constant and near Planckian for normal sized N. It has curvature invariants of order $O(\frac{1}{Nl_P{}^2})$, as we read off from the γ in the denominator. When we consider large N limit, or semi-classical limit, those curvature invariants are no longer Planckian, and therefore, our assumption still holds.

Note that the first two cases, $a_S(r)$ and $a_\eta(r)$, are still finite at $\hbar \to 0$ limit, meaning that their classical descriptions exist. However, the latter two cases, $a_{den}(r)$ and $a_{neg}(r)$, are singular at $\hbar \to 0$ limit. That suggests they exist due to quantum effects, and are non-perturbative in $\hbar$.

The reason why Eq. (5.1.13) is named nonphysical is because within the physical domain of η, the value of K in Eq. (5.1.15) is always negative, making the mass given in Eq. (3.1.2) always negative. That means $a(r) < 0$ which violates the physical conditions mentioned in Sec. 3.3.

In the following, we are going to solely focus on the physical ones.

5.2 Linearized Equations

In this section, we focus on the true solutions that are near the physical asymptotic solutions, which are summarized in Sec. 5.1. That means we are going to substitute in to the $a(r)$-

doi:10.6342/NTU202302515

equation Eq. (4.5.1) the ansatz

$$a(r) = a_{asymp}(r) + \epsilon f(r), \tag{5.2.1}$$

where $f(r) = a_{asymp}(r)\mathcal{D}(r)$, and solve it up to $O(\epsilon)$, which are linearized differential equations. Note that in the following, we use the same subscript to denote which asymptotic solution we are expanding around. For example, differential equation of $f_S(r)$ is expanded around $a_S(r)$.

The following are the equation:

$$f_S''(r) - \frac{2(\eta-1)}{(2-\eta)r} f_S'(r) = 0 \tag{5.2.2}$$

$$\begin{aligned}\left(\eta^2-\eta+1\right) f_\eta''(r) + \frac{(\eta-1)\left(\eta^2-\eta+1\right)}{r} f_\eta'(r) \\ + \frac{\eta(\eta-1)(2\eta-1)\left(\eta^2-\eta+1\right)}{(2-\eta)r^2} f_\eta(r) = 0\end{aligned} \tag{5.2.3}$$

$$-\frac{3\eta^2(2\gamma(2-\eta))}{16\gamma^2(2-\eta)} \bar{f}_{den}''\left(r^2\right) - \frac{9\gamma\eta^3(4-\eta)}{32\gamma^3(2-\eta)} \bar{f}_{den}'\left(r^2\right) - \frac{27\eta^5}{64\gamma^3(2-\eta)} \bar{f}_{den}\left(r^2\right) = 0, \tag{5.2.4}$$

where the bar in the last equation is to emphasize the derivative is $\frac{d}{dr^2}$ not $\frac{d}{dr}$. These equation can be solved as follows.

doi:10.6342/NTU202302515

f_S-equation

Eq. (5.2.2) can be rewritten as

$$0 = \left(D - \frac{2(\eta-1)}{(2-\eta)r}\right) D f_S(r), \tag{5.2.5}$$

where $D = \frac{\mathrm{d}}{\mathrm{d}r}$. The equation then can be solved by hand in this form from the left-most operator, $\left(D - \frac{2(\eta-1)}{(2-\eta)r}\right)$, to the right. Then we obtain

$$f_S(r) \in \mathrm{span}\left\{1, r^{\frac{\eta}{2-\eta}}\right\}. \tag{5.2.6}$$

f_η-equation

For Eq. (5.2.3), we observe that it can be solved with power ansatz, that is, $f(r) = r^k$, to obtain characteristic equation, and solve for k.

The form of the characteristic equation is

$$\left(\eta^2 - \eta + 1\right) k(k-1) + \frac{(\eta-1)\left(\eta^2-\eta+1\right)}{r} k + \frac{\eta(\eta-1)(2\eta-1)\left(\eta^2-\eta+1\right)}{(2-\eta)r^2} = 0, \tag{5.2.7}$$

which is just a quadratic equation in k, and the solution is

$$k = \frac{1}{2}\left(2 - \eta \pm \sqrt{9\eta^2 + \frac{24}{\eta-2} + 16}\right). \tag{5.2.8}$$

Hence the general solution for $f_\eta(r)$ is

$$f_\eta(r) \in \mathrm{span}\left\{r^{\frac{1}{2}\left(2-\eta\pm\sqrt{9\eta^2+\frac{24}{\eta-2}+16}\right)}\right\}. \tag{5.2.9}$$

doi:10.6342/NTU202302515

f_{den}-equation

The f_{den} case is the easiest one to solve, since it can directly be solved with the ansatz for characteristic equation, $f_{den}(t) = e^{-st}$, of Eq. (5.2.4). The solutions are

$$s = \frac{3\eta}{2\gamma}, \frac{3\eta^2}{4\gamma(2-\eta)}. \tag{5.2.10}$$

Hence,

$$f_{den}(r) \in \text{span}\Big\{e^{-sr^2} : s = \frac{3\eta}{2\gamma}, \frac{3\eta}{4\gamma(2-\eta)}\Big\}. \tag{5.2.11}$$

Summary of Linearized Equations

Before proceeding, we give a short summary to results obtained int this section. As mentioned in the beginning of the chapter, we are measuring the difference between asymptotic solutions to the true solutions with $\mathcal{D}(r) = \frac{f(r)}{a_{asymp}(r)}$. In the following, when we mention difference increases as r grows, it means $\mathcal{D}(r)$ increases as r grows given the corresponding asymptotic solution.

First, we talk about the a_S case. Since $f_S(r)$ is some function spanned by 1 and $r^{\frac{\eta}{2-\eta}}$, the difference increases as r grows. That means $a_S(r)$ is not a stable fixed point in as r increases in the phase space of the $-$ branch equation. Note that even though there is some ambiguity at $O(\epsilon)$ level that whether the basis 1 creates instability in the phase space, we can check it numerically in Sec. 5.3. It turns out it is indeed creating instability.

Next, we focus on a_η case. Within the domain of η (see Sec. 3.2, both of the bases, $r^{\frac{1}{2}\left(2-\eta\pm\sqrt{9\eta^2+\frac{24}{\eta-2}+16}\right)}$, have power smaller than 1, making the form of $\mathcal{D}(r) \sim r^{-c}$ where c is some positive real number. Hence, given an initial data around $a_\eta(r)$, it will eventually stabilize at $a_\eta(r)$ as r increases in the phase space of $-$ branch equation.

doi:10.6342/NTU202302515

The last case is $a_{den}(r)$. It is clear that this represents a fixed point in the phase space of + branch equation, since both of $f_{den}(r)$'s bases are Gaussians, forcing $\mathcal{D}(r)$ must decrease as r grows.

These features are going to be summarized graphically in Fig. 5.1 in the next section.

5.3 Structure of Solution Space

After solving the $a(r)$-equation Eq. (4.5.1) asymptotically in previous sections, here we discuss the solutions, which are classified by the nearest asymptotic solutions, numerically.

First of all, to solve Eq. (4.5.1) numerically, we have to make the equation itself non-singular, so that the numerical solver can update the highest order term (in this case, $a''(r)$) without ambiguity. That means to adopt numerical method we should use Eq. (4.5.2) instead of Eq. (4.5.1). In Eq. (4.5.2), we have 2 branches of equations, the + and − branch equations.

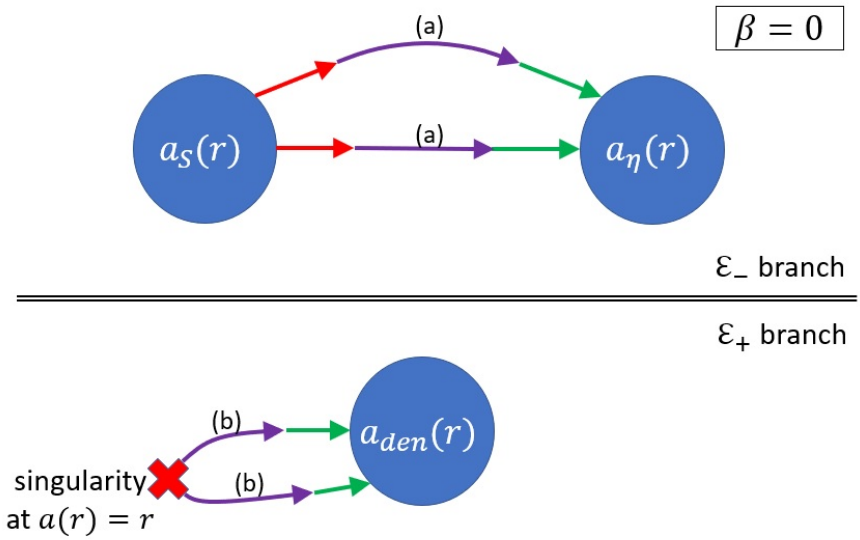

Figure 5.1: The flowchart representing the structure of the solution space of $\beta = 0$. Red (green) arrows represent relevant (irrelevant) directions. The transitions (a) and (b) correspond to Fig.5.2 and Fig.5.3, respectively.

doi:10.6342/NTU202302515

By substituting the forms of $a_S(r)$, $a_\eta(r)$, and $a_{den}(r)$ into both equations, we find the first two satisfy the $-$ branch equation, while the last one solves the $+$ branch equation. Hence we obtain three blue blobs in Fig. 5.1 and a doubled line separation, which indicates the upper solutions are obtained from the $-$ branch equation, while the lower one is obtained from the $+$ branch equation. Note that the vectors around each solutions, classified by asymptotic solutions, represents whether an initial data around them will be led toward or away from the asymptotic behaviors, which are discussed in Sec. 5.2. Red vector means having growing deviation, while the green one denotes decreasing in deviation.

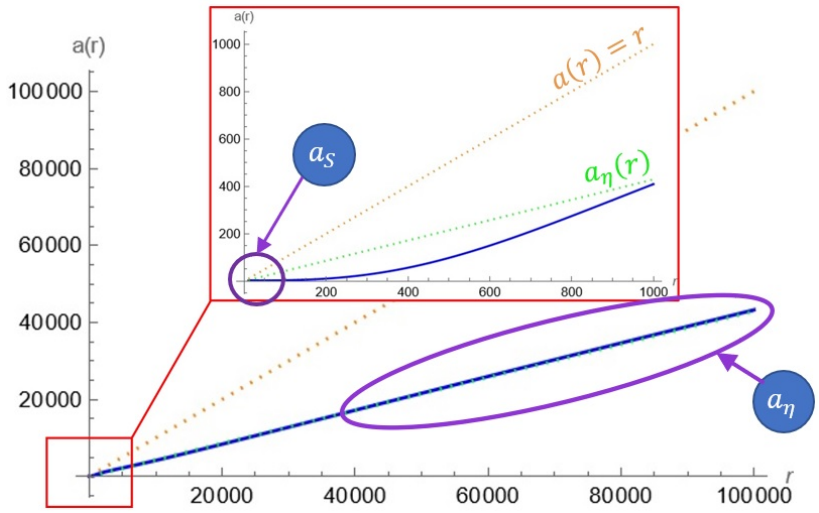

Figure 5.2: Transition (a) in Fig. 5.1. Note that orange dotted line represents $a = r$, and green dotted line is $a_\eta(r)$.

The remaining tasks are to find where those red vectors go as r increases, and where do those green vectors comes from in the opposite direction. They are represented by purple lines connecting among vectors or singularity as shown in Fig. 5.1. For example, the transition denoted as (a) represents that given an initial data around $a_S(r)$ and we evolve it with $-$ branch equation (denoted around doubled line separation), it will ends up at $a_\eta(r)$. We give a numerical example of it in Fig. 5.2. Notice that this transition process from a_S to

doi:10.6342/NTU202302515

a_η requires a long distance of r. As for transition (b), the numerical example is shown in Fig. 5.3. Here we start from larger r with near-$a_{den}(r)$ values, and evolve to smaller r with $+$ branch equation. Note that, at smaller r, we hit $a = r$ singularity, so we do not identify it as $a_{den}(r)$. This is checked in Fig. 5.4, where the curvature is singular at small r, not some constant value as Eq. (5.1.12) suggested. Hence, we complete the flowchart in Fig. 5.1.

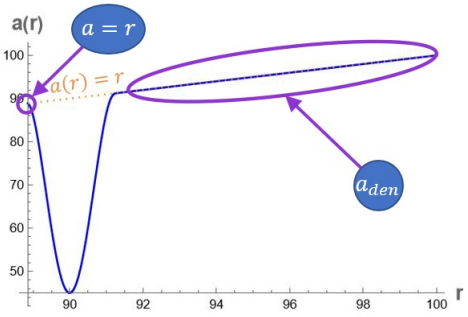

Figure 5.3: Transition (b) in Fig. 5.1. Note that orange dotted line represents $a = r$, and green dotted line is $a_\eta(r)$.

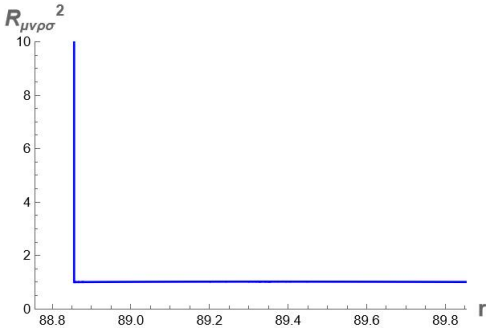

Figure 5.4: $R^{\mu\nu\alpha\beta}R_{\mu\nu\alpha\beta}$ for Fig. 5.3 diverges at the point satisfying $a(r) = r$.

Note that it is an illusion from these numerical results that we can only have these 2 types of solutions (Figs. 5.2 and 5.3). Since these are obtained from subjecting to single branch of equation, we, in fact, still have the freedom to switch to the other branch at any r, during evolving the data. The resulting solution must as well be a solution to the $a(r)$-equation, since the solution satisfies either $+$ or $-$ branch of equation, which are derived from $a(r)$-equation! This provides an infinite number of free parameters, and suggesting a wide varieties of internal geometries given an ADM mass as boundary condition.

doi:10.6342/NTU202302515

Chapter 6

Internal Geometries and Entropy

In this chapter, we are going to discuss the internal geometries of quantum black holes based on our analysis in chapter 5 under the criteria mentioned in Secs. 3.2 and 3.3.

6.1 Simplest Internal Structure

To begin with, we construct the simplest possible internal geometry in this section.

As we have discussed in Sec. 3.3, since we expect $r_{sur} \approx a_0$, the only possible asymptotic behavior at $r \lesssim r_{sur}$ is $a_{den}(r)$. That means we must have a_{den} at $r \lesssim r_{sur}$ and Schwarzschild at $r \geq r_{sur}$ with suitable junction condition at $r = r_{sur}$[1]. For other cases, they are far from the condition to be near $a = r$, which is the requirement to connect at $r = r_{sur}$ to external geometry. At the same time, $a_{den}(r)$ predicts $r_{sur} \approx a_0 + \frac{2\gamma}{3\eta^2 a_0}$ as shown in Eq. (4.4.14), suggesting a horizonless black hole.

For the simplest possible black hole from what we have so far, it is represented as in Fig. 6.1. Starting from $r > r_{sur}$, we have Schwarzschild metric with Schwarzschild radius a_0. As we cross $r = r_{sur}$, we have $a \approx r$ all the way down to $r_0 \approx 0$ with slope about 0, which

[1]Here we only assume that they must be continuously connected, and this is some topic for future work.

doi:10.6342/NTU202302515

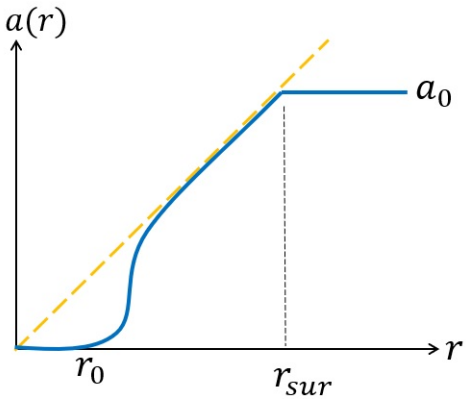

Figure 6.1: Plot of $a(r)$ for Fig. 6.2. Note that at $r < r_0$, the metric described by a_S, or well-approximated by Schwarzschild metric, see Sec. 4.6 for more details.

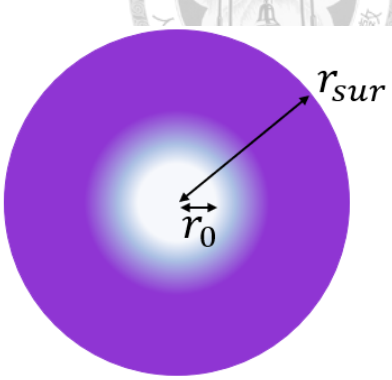

Figure 6.2: The simplest internal configuration. The darker the (purple) color is, the higher the energy density is.

has the behavior of the lowest point in Fig. 5.3. Then, to avoid hitting singularity, we switch to $-$ branch equation and connect to a_S with $c_0 \approx 0$, or simply Minkowski metric. This seemingly extra switching and connection to a_S not a_η are necessary due to the following reasons. First, if we do not switch to the other branch of equation at small r, the subleading term will become large and lead our solution to hit $a = r$ singularity. Next, after switching to $-$ branch equation, we know from Fig. 5.1, $a_S(r)$ is stable in r decreasing direction, while $a_\eta(r)$ is not. One may argue that we have switch branch at larger r_0 with slope coinciding with that of a_η. However, this case we will unavoidably require a second (even a third) switching to prevent singularities. That is because when connecting to a_η it will eventually go to a_S at smaller r with $c_0 \neq 0$, and hit $a = r$ singularity. To prevent such singular behavior extra switching is required, and then it is no longer simpler than the case we are presenting in the first place. Hence, we can argue the solution represented in Fig. 6.1 is the simplest possible internal structure that is physical (see Sec. 3.3). Note that in configuration space, it will look something like in Fig. 6.2, where we use darker purple to denote higher energy density.

doi:10.6342/NTU202302515

6.2 Internal Structures, Micro-canonical Ensemble, Entropy, and Next

In this section, we are going to discuss a more complicated internal structure than the one mentioned in Sec. 6.1.

As mentioned in Sec. 5.3, the infinite variety of internal structure stems from uncontrolled switching between different branches of equations. At the same time, we have discussed why a_S is more favorable than a_η when switching to $-$ branch in Sec. 6.1. We can conclude that to construct a general solution to the $a(r)$-equation Eq. (4.5.1), we can simply consider combinations among a_S and a_{den}, where a_S is nothing more than Schwarzschild (see discussion in Sec. 4.6. Hence, a more complicated structure can be viewed as inserting vacuum regions into the simplest internal structure as shown in Fig. 6.1.

In Fig. 6.3, we show examples from the argument above with different number of vacuum insertion. Interestingly, as the number of substituted vacua ($a(r) \sim const.$) increases, that is, starting from the left, center, and then to the right figures, the solution becomes increasingly closer to the simplest internal structure shown in Fig. 6.1. Hence, we say that the simplest internal structure shown in Fig. 6.1 can be used to approximate solutions with the most number of switching.

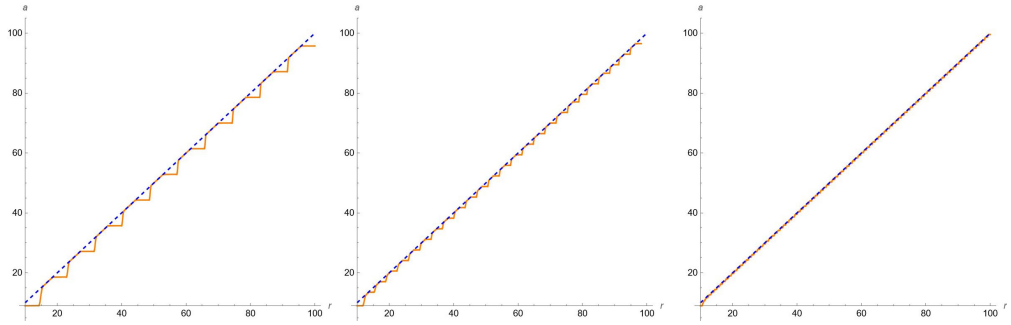

Figure 6.3: Examples for different number of vacuum insertions. From left to right, we increase the number of insertions, and it turns out it is approaching a_{den}.

doi:10.6342/NTU202302515

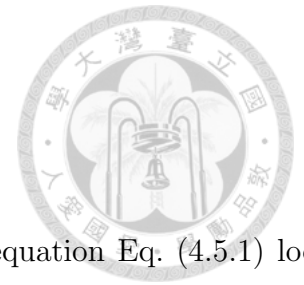

Entropy

Now, we have the complete picture of how solutions to the $a(r)$-equation Eq. (4.5.1) look like. Let's discuss entropy from this picture.

In analogy to microcanonical ensemble [50], we define every possible internal structure to be a microstate of our system, and apply the postulate of "*equal a priori probabilities*". Then, to calculate black hole entropy, we first assume the black hole is in equilibrium, that is, immersing it in a radiation bath of temperature T_0.[2] Since it is now in equilibrium, we can calculate macroscopic states from the most probable set in the state space. At the same time, we know states in the most probable set can be approximated by the simplest internal structure. Hence, it is reasonable to use the simplest internal structure to estimate entropy of a black hole.

Since we know the simplest internal structure is filled with highly dense region, a_{den}, from r_0 to $r_{sur} \approx a_0$, we can estimate the number of switching with its related results. Due to the fact that the solutions in the most probable states are well-approximated by a_{den}, every vacuum insertion can be regarded as small deviation from it. Fortunately, we know how to describe those small deviations from highly dense regions, that is, to use f_{den}! In Eq. (5.2.11), we know f_{den} is a function in the span of Gaussians e^{-sr^2} where $s = \frac{3\eta}{2\gamma}, \frac{3\eta}{4\gamma(2-\eta)}$, suggesting a natural size of switching to be the width of these Gaussians, that is,

$$\sigma = \sqrt{\frac{4\gamma}{3\eta}}, \sqrt{\frac{8\gamma(2-\eta)}{3\eta}}, \tag{6.2.1}$$

where σ's are the standard deviation of the Gaussians[3]. To consider the largest possible number of switching, we consider distributing the former σ, which has smaller value, over

[2] We don't specify the actual value for T_0, since it is not affecting our statement.

[3] The standard form for Gaussian distribution is $\frac{1}{\sigma\sqrt{2\pi}} e^{-\frac{1}{2}\left(\frac{x-\mu}{\sigma}\right)^2}$, where μ is the mean and σ is the standard deviation.

doi:10.6342/NTU202302515

region in between r_0 and r_{sur}. Hence, the largest number of switching is

$$n_{max} = \frac{l_{size}}{\sigma_{min}} \tag{6.2.2}$$

where

$$\begin{aligned} \sigma_{min} &= \min\left(\sqrt{\frac{4\gamma}{3\eta}}, \sqrt{\frac{8\gamma(2-\eta)}{3\eta}}\right) = \sqrt{\frac{4\gamma}{3\eta}} \\ l_{size} &= \int_{r_0}^{r_{sur}} dr \left(\sqrt{g_{rr}(r)}\right) = \sqrt{\frac{3\eta^2}{8\gamma}}\left(r_{sur}^2 - r_0^2\right) \end{aligned} \tag{6.2.3}$$

is the proper length from $r = r_0$ to $r = r_{sur}$, and $\sigma_2 = \sqrt{\frac{4\gamma}{3\eta}}$, making

$$\begin{aligned} n_{max} =& \left(\sqrt{\frac{3\eta^2}{8\gamma}}\left(r_{sur}^2 - r_0^2\right)\right)\left(\sqrt{\frac{3\eta}{4\gamma}}\right) \\ =& \sqrt{\frac{9\eta^3}{32}}\frac{r_{sur}^2 - r_0^2}{\gamma}. \end{aligned} \tag{6.2.4}$$

Also, consider a double switching structure that is a_{den} sandwiched by vacua on both sides. For the matter content of a_{den}, this structure has a free choice among N matter fields to choose from. Therefore, per double switching, we have N bits[4] of information, making the total entropy S to be approximately

$$\begin{aligned} S =& N \times \frac{n_{max}}{2} \\ =& \sqrt{\frac{9\eta^3}{128}}\left({r_{sur}}^2 - {r_0}^2\right)\frac{N}{\gamma} \\ \sim& O({a_0}^2), \end{aligned} \tag{6.2.5}$$

[4]For example, we label N matter fields from 1 to N, and we use a sequence of 0's and 1's of length N to denote the choice of matter content. That is, 1 represents to select the field, and 0 means not to. Then the full matter content is described the binary sequence.

doi:10.6342/NTU202302515

which suggests an area law for entropy. Note that above we use the fact that $r_{sur} \approx a_0$, $r_0 \approx 0$, and $\gamma \sim N$.

Even though this object we have been discussing is horizonless, it has entropy proportional to area, which is a characteristic of black holes. This means without loss of generality, we shall identify such objects as black holes.

To brief about this black hole, we state some results we derived related to it. In region between Schwarzschild radius (a_0) and $r_{sur} \approx a_0 + O({a_0}^{-1})$, this type of black hole is filled with high energy density matter, replacing Schwarzschild radius at $r = a_0$ with a surface of matter at $r = r_{sur}$; it has firewall at $a = r$; This types of horizonless black holes is a totally quantum object, since it does not exists in $\hbar \to 0$ limit.

Next

After proving this object to be a candidate of the Schwarzschild black hole itself, we can ask something that we could not ask, or does not make sense, before. That is, "how does the internal structure evolve with time?"

In this picture, this question is nontrivial. Since the internal metric is not Schwarzschild metric, so it can have time-dependence. Also, their stability in time still remains unknown, since we have not discuss any dynamics of the setup. As we know more about the fate of this type of black hole, we should be able to understand more about other proposals as well. For example, since firewall is a built-in substructure of this black hole, we can test this proposal in more details. Also, it should inspire the direction of fuzzball, which suggests building area law from microstates represented by strings. Thus, in the next chapter, we are going to give a simple proof in order to suggest the time-dependence is indeed nontrivial, and requires more research.

doi:10.6342/NTU202302515

Chapter 7

Time-dependence: A First Leap

In this chapter, we are going to take a first leap to solve the time-dependence of our setup. That is, we solve the same system, including equation of state Eq. (4.0.3), but this time we adopt the time-dependent metric, that is,

$$ds^2 = -\frac{e^{A(t,r)}}{B(t,r)}dt^2 + B(t,r)dr^2 + r^2 d\Omega_2. \tag{7.0.1}$$

After solving a simplified version of the equation, we find it is suggesting the internal geometry, which represents Schwarzschild black hole itself, is time dependent.

In the following, let's first find the simplified equation, try to solve it, and prove the above statement.

In general, this is almost an impossible task, due to the nonlinear nature of Einstein equations. Hence, we are going to consider the following ansatz

$$a(t,r) = a_{static}(r) + \epsilon b(t,r), \tag{7.0.2}$$

where $a_{asymp}(r)$ is the asymptotic behaviors we obtained in the static analysis, and ϵ here is

doi:10.6342/NTU202302515

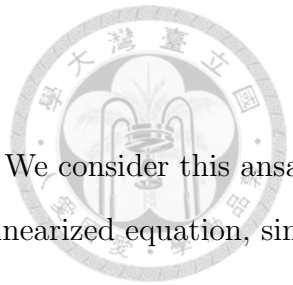

just a small number, which has nothing to do with the former one. We consider this ansatz and solve the equation up to $O(\epsilon)$. That means we solve the time-linearized equation, since there is not going to be any time-related terms to be mixed[1].

The equation, in the canonical form of wave equation, takes the following form,

$$\ddot{v}(t,s) = v''(t,s) - U_{eff}(s, f(s))v(t,s), \tag{7.0.3}$$

where the function $b(s)$ is replaced with a product of 2 functions $f(s)v(t,s)$ to get the canonical form, $s = s(r)$ is a new coordinate mapped from r with the relation

$$\frac{\partial s}{\partial r} = \sqrt{\frac{\eta}{2-\eta}} B(r) e^{-\frac{A(r)}{2}}, \tag{7.0.4}$$

where $A(r), B(r)$ are obtained from the static result, and the form of f and U_{eff} are recorded in Appendix A. The advantage of this form is the ease of reading of dispersion relation, meaning after Fourier transforming t and r we have

$$\omega^2 = k^2 + U_{eff}, \tag{7.0.5}$$

where ω and k are conjugate to t and r respectively. Since the question we want to answer is whether the time dependence of the interior geometries is trivial, we can use this dispersion relation to answer. The idea is simple. For given position r, we can solve for ω for all k. If ω turns out to be complex, that means the solution bases responsible for time dependent part are exponentials, which increases with time exponentially, creating instability to the system.

In practice, since the form of U_{eff} is too complicated, see Appendix A, we cannot do this qualitatively. Instead, we restore the power of numerical simulations, and solve the

[1]That is because the appearance of t in a term of the equation is the same as the order of ϵ. Hence, terms such as $b(t,r)\partial_t b(t,r)$ is not going to appear in the equation.

doi:10.6342/NTU202302515

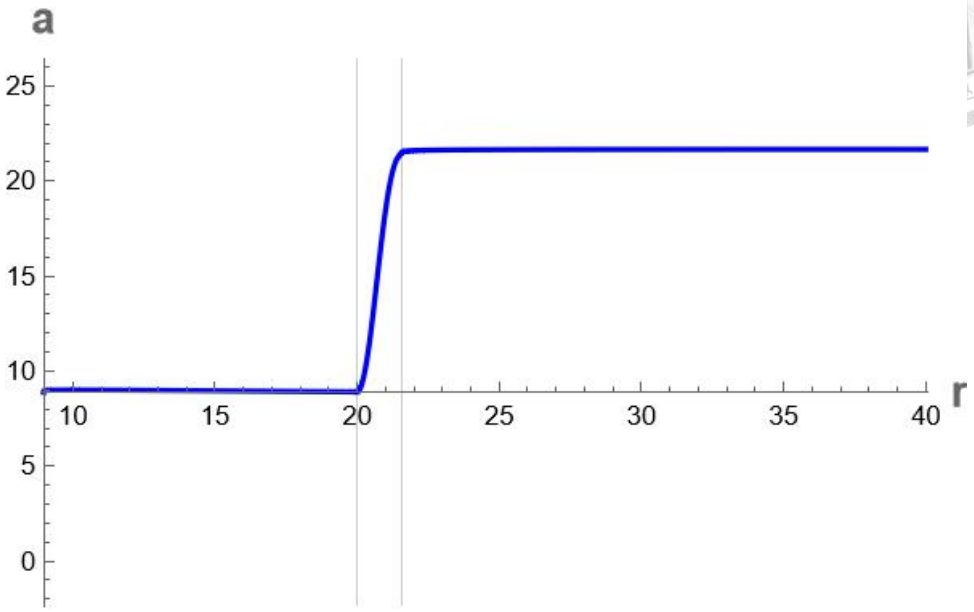

Figure 7.1: $a - r$ plot for the chosen static solution for simulation, which has the form a_{den} sandwiched by Schwarzschild metrics, and the switching, or junction, positions are donoted by the vertical lines at $r = 20$ and $r = 21.6$. Note that the window for simulation is set to be $9 \leq r \leq 40$.

system under a simple static solution, that is, a high energy density region, described by a_{den}, sandwiched by Schwarzschild metrics, see Fig. 7.1.

For simulation, we also need to supply the initial and boundary conditions for $b(t, r)$. We attempt to send a small perturbation into the a_{den} region from larger r. Hence, the initial conditions are set to be Gaussian with center located at $r > 21.6$ with negative velocities ($\partial_t b(0, r) < 0$), see Fig. 7.2 for initial profile for b. For boundary condition, as a trial, we adopt Dirichlet boundary condition at $r = 9, 40$, the boundary of the solving window. We summarize the full result in Appendix B. Here we only show one of the time slice in Fig. 7.3 to show there the wavepacket indeed accumulates at the junction, suggesting an instability.

doi:10.6342/NTU202302515

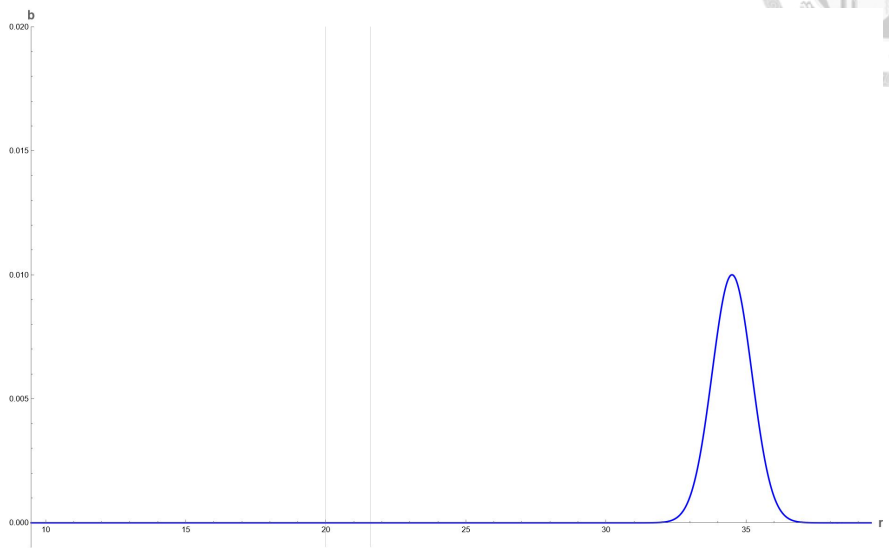

Figure 7.2: Initial profile of b for simulations. The Gaussian is centered at $r = 35$ with standard deviation $\sigma = 1$, and the vertical lines denote the junction positions.

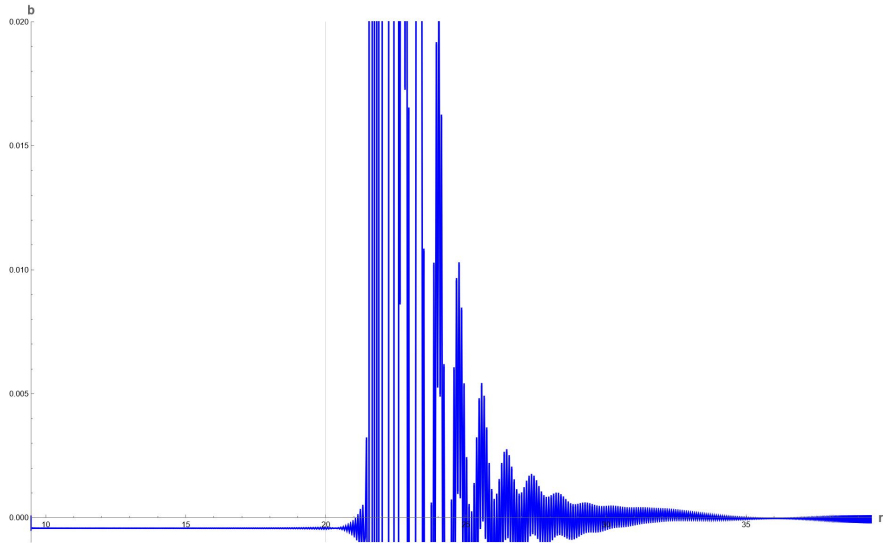

Figure 7.3: After evolving the initial conditions (Fig. 7.2) with the time dependent equation, we find the wavepacket indeed are trapped at $r = 21.6$, which is one of the junction positions. This suggests an instability of junction, and thus it should have nontrivial time dependence.

doi:10.6342/NTU202302515

Chapter 8

Summary

In this thesis, we have considered Schwarzschild black holes with back-reactions due to quantum effects. By approximating the matter fields with those with conformal symmetry at classical level, implying 4 dimensional Weyl anomaly at quantum level, we solve the semi-classical Einstein equation subjected to a suitable equation of state[1].

We first analyze the system with time-independent metric. Through the asymptotic solutions of this static system, we find a simple classification[2] of the behavior of solutions. The behavior with highest energy density, a_{den}, turns out to be the most nontrivial one, and provides the most information.

First, it cannot be obtained at perturbative (in $\hbar$) level, so the usual treatment with perturbation analysis is not good enough to sense this behavior.

Second, it gives a prediction on the size of the region where semi-classical physics cannot be ignored, meaning where Schwarzschild metric is not good enough. Interestingly, such region is suggested to be slightly larger than Schwarzschild radius (more precisely, $r \leq a_0 + O({a_0}^{-1}) \equiv r_{sur}$, where a_0 is the Schwawrzschild radius), enclosing the black hole itself.

[1]This is justified in chapter 4

[2]Only 3 classes are sufficient: low, medium, high energy densities.

doi:10.6342/NTU202302515

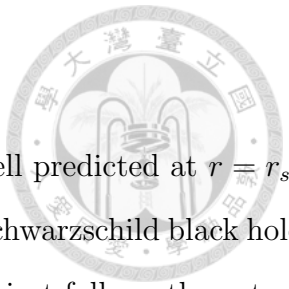

The extended region from a_0 is highly dense where the surface is well predicted at $r = r_{sur}$. Hence, we derive a horizonless object, inspired from expectation of Schwarzschild black holes.

Third, from the analysis of a_{den}, we derive the entropy of this object follows the entropy area law. That provides an evidence that this object is a black hole, or more precisely, Schwarzschild black hole itself.

The calculation on entropy is based on our full understanding of the static solutions. We find that given the mass of a black hole, its internal geometry is not unique. That incentivizes us to apply the setup of microcanonical ensemble in statistical mechanics to calculate entropy. By defining each possible internal geometry as a microstate, we find the most probable states can be approximated by those with most of the region covered by a_{den}. Hence through the characteristic of a_{den} we predict the area law for entropy. Note that this picture is very similar to fuzzball with the main difference that we are not considering microstates from strings but classical geometries.

Now since we can regard Schwarzschild black hole itself as an object without singularities, we can test whether it is still having no dynamics, that is, always time independent. We perform an simulation on a simple example to understand the time dependent nature of this black hole, and the result suggests such object has nontrivial time dependence.

Meanwhile, we find our black hole has firewalls as its substructure internally. Therefore, by analyzing more about the time dependence of the system, we should gain more inspiration on firewalls, fuzzballs, and other proposals.

doi:10.6342/NTU202302515

Bibliography

[1] S. W. Hawking, Commun. Math. Phys. **43** (1975), 199-220 [erratum: Commun. Math. Phys. **46** (1976), 206]

[2] N. D. Birrell and P. C. W. Davies, *"Quantum Fields in Curved Space,"* Cambridge Univ. Press, 1984

[3] L. Parker, Phys. Rev. Lett. **21**, 562-564 (1968)

[4] R. M. Wald, *"Quantum Field Theory in Curved Space-Time and Black Hole Thermodynamics,"* University of Chicago Press

[5] R. M. Wald, *"General Relativity,"* Chicago Univ. Pr., 1984

[6] H. Kawai and Y. Yokokura, Phys. Rev. D **105**, no.4, 045017 (2022) [arXiv:2108.02242 [hep-th]].

[7] H. Kawai and Y. Yokokura, Universe **6**, no.6, 77 (2020) [arXiv:2002.10331 [hep-th]].

[8] H. Kawai and Y. Yokokura, Universe **3**, no.2, 51 (2017) [arXiv:1701.03455 [hep-th]].

[9] H. Kawai and Y. Yokokura, Phys. Rev. D **93**, no.4, 044011 (2016) [arXiv:1509.08472 [hep-th]].

doi:10.6342/NTU202302515

[10] H. Kawai and Y. Yokokura, Int. J. Mod. Phys. A **30**, 1550091 (2015) [arXiv:1409.5784 [hep-th]].

[11] H. Kawai, Y. Matsuo and Y. Yokokura, Int. J. Mod. Phys. A **28**, 1350050 (2013) [arXiv:1302.4733 [hep-th]].

[12] P. M. Ho, Class. Quant. Grav. **34**, no.8, 085006 (2017) [arXiv:1609.05775 [hep-th]].

[13] S. W. Hawking, Nature **248**, 30-31 (1974)

[14] S. P. Robinson and F. Wilczek, Phys. Rev. Lett. **95**, 011303 (2005) [arXiv:gr-qc/0502074 [gr-qc]].

[15] P. M. Ho, H. Kawai, H. Liao and Y. Yokokura, [arXiv:2307.08569 [hep-th]].

[16] V. Cardoso and P. Pani, Living Rev. Rel. **22**, no.1, 4 (2019) [arXiv:1904.05363 [gr-qc]].

[17] S. W. Hawking and G. F. R. Ellis, *"The Large Scale Structure of Space-Time,"* Cambridge University Press, 2023

[18] J. D. Bekenstein, Lett. Nuovo Cim. **4**, 737-740 (1972)

[19] B. L. B. Hu and E. Verdaguer, *"Semiclassical and Stochastic Gravity: Quantum Field Effects on Curved Spacetime,"* Cambridge University Press, 2020

[20] S. J. Avis and C. J. Isham, Nucl. Phys. B **156**, 441-455 (1979)

[21] B. S. DeWitt, C. F. Hart and C. J. Isham, Physica A **96**, no.1-2, 197-211 (1979)

[22] J. S. Dowker and G. Kennedy, J. Phys. A **11**, 895 (1978)

[23] E. Elizalde, Int. J. Mod. Phys. A **27**, 1260005 (2012) [arXiv:1205.7032 [math-ph]].

[24] L. H. Ford, Phys. Rev. D **14**, 3304-3313 (1976)

doi:10.6342/NTU202302515

[25] L. H. Ford, Phys. Rev. D **11**, 3370-3377 (1975)

[26] J. S. Dowker and R. Banach, J. Phys. A **11**, 2255 (1978)

[27] W. Israel, Phys. Lett. A **57**, 107-110 (1976)

[28] L. Parker, Phys. Rev. D **12**, 1519-1525 (1975)

[29] R. M. Wald, Commun. Math. Phys. **45**, 9-34 (1975)

[30] J. B. Hartle and S. W. Hawking, Phys. Rev. D **13**, 2188-2203 (1976)

[31] L. Parker and S. A. Fulling, Phys. Rev. D **9**, 341-354 (1974)

[32] S. A. Fulling and L. Parker, Annals Phys. **87**, 176-204 (1974)

[33] S. A. Fulling, L. Parker and B. L. Hu, Phys. Rev. D **10**, 3905-3924 (1974)

[34] B. L. Hu, Phys. Lett. A **71**, 169-173 (1979)

[35] Y. B. Zeldovich and A. A. Starobinsky, Zh. Eksp. Teor. Fiz. **61**, 2161-2175 (1971)

[36] B. L. Hu, Phys. Rev. D **18**, 4460-4470 (1978)

[37] B. L. Hu, Phys. Rev. D **9**, 3263-3281 (1974)

[38] J. S. Dowker and R. Critchley, Phys. Rev. D **13**, 3224 (1976)

[39] S. W. Hawking, Commun. Math. Phys. **55**, 133 (1977)

[40] E. Elizalde, S. D. Odintsov, A. Romeo, A. A. Bytsenko and S. Zerbini, *"Zeta regularization techniques with applications,"* World Scientific Publishing, 1994

[41] D. V. Vassilevich, Phys. Rept. **388**, 279-360 (2003) [arXiv:hep-th/0306138 [hep-th]].

doi:10.6342/NTU202302515

[42] R. M. Wald, Phys. Rev. D **17**, 1477-1484 (1978)

[43] R. M. Wald, Commun. Math. Phys. **54**, 1-19 (1977)

[44] P. M. Ho, Y. Matsuo and S. J. Yang, Class. Quant. Grav. **37**, no.3, 035002 (2020) [arXiv:1903.11499 [hep-th]].

[45] P. M. Ho, Nucl. Phys. B **909**, 394-417 (2016) [arXiv:1510.07157 [hep-th]].

[46] P. M. Ho, H. Kawai, H. Liao and Y. Yokokura, [arXiv:2307.08569 [hep-th]].

[47] E. Poisson, *"A Relativist's Toolkit: The Mathematics of Black-Hole Mechanics,"* Cambridge University Press, 2009

[48] M. J. Duff, J. Phys. A **53**, no.30, 301001 (2020) [arXiv:2003.02688 [hep-th]].

[49] D. M. Hofman and J. Maldacena, JHEP **05**, 012 (2008) [arXiv:0803.1467 [hep-th]].

[50] R. K. Pathria, *"Statistical Mechanics,"* Butterworth-Heinemann, 1996

doi:10.6342/NTU202302515

Appendix A

U_{eff}

In this appendix, we give the full form of U_{eff} mentioned in chapter 7 as a function of r. It takes the form as follows:

$$U_{eff}(r) = \frac{U_{eff,n}(r)}{U_{eff,d}(r)}, \tag{A.0.1}$$

where

$$\begin{aligned} U_{eff,n}(r) =& a_{21}(r)A''(r) + a_{12}(r)A'(r)^2 + a_{11}(r)A'(r) \\ &+ b_{31}(r)B'''(r) \\ &+ b_{23}(r)B''(r)^3 + b_{22}(r)B''(r)^2 + b_{21}(r)B''(r) \\ &+ b_{16}(r)B'(r)^6 + b_{15}(r)B'(r)^5 + b_{14}(r)B'(r)^4 \\ &+ b_{13}(r)B'(r)^3 + b_{12}(r)B'(r)^2 + b_{11}(r)B'(r) \\ &+ c_{00}(r) \end{aligned} \tag{A.0.2}$$

doi:10.6342/NTU202302515

and

$$
\begin{aligned}
U_{eff,d}(r) =& 16\eta^3 r^2 B(r)^4 \\
& \Big(-2\gamma(\eta-2)(2\eta-1)r^2 B'(r)^2 \\
& + 2B(r)^2 \left(\gamma(\eta-4)rB'(r) - 2\left(\gamma(\eta+1)^2 - 3\alpha\eta^2\right)\right) \\
& + 2\gamma r B(r)\left((\eta-2)\eta r B''(r) - \left(2\eta^2+\eta-4\right)B'(r)\right) \\
& + B(r)^3\left(4\gamma(\eta(\eta+2)+2) + 3\eta^2\left(r^2-4\alpha\right)\right) - 4\gamma B(r)^4\Big)^2,
\end{aligned}
\tag{A.0.3}
$$

where $A(r)$ and $B(r)$ depends on the chosen static solutions, and

$$
\begin{aligned}
a_{21}(r) =& 4(\eta-2)\eta^2 r^2 e^{A(r)} B(r)^2 \\
& \Big(-2\gamma(\eta-2)(2\eta-1)r^2 B'(r)^2 \\
& + 2B(r)^2 \left(\gamma(\eta-4)rB'(r) - 2\left(\gamma(\eta+1)^2 - 3\alpha\eta^2\right)\right) \\
& + 2\gamma r B(r)\left((\eta-2)\eta r B''(r) - \left(2\eta^2+\eta-4\right)B'(r)\right) \\
& + B(r)^3\left(4\gamma(\eta(\eta+2)+2) + 3\eta^2\left(r^2-4\alpha\right)\right) - 4\gamma B(r)^4\Big)^2,
\end{aligned}
\tag{A.0.4}
$$

$$
\begin{aligned}
a_{12}(r) =& (\eta-2)\eta^2 r^2 e^{A(r)} B(r)^2 \\
& \Big(-2\gamma(\eta-2)(2\eta-1)r^2 B'(r)^2 \\
& + 2B(r)^2 \left(\gamma(\eta-4)rB'(r) - 2\left(\gamma(\eta+1)^2 - 3\alpha\eta^2\right)\right) \\
& + 2\gamma r B(r)\left((\eta-2)\eta r B''(r) - \left(2\eta^2+\eta-4\right)B'(r)\right) \\
& + B(r)^3\left(4\gamma(\eta(\eta+2)+2) + 3\eta^2\left(r^2-4\alpha\right)\right) - 4\gamma B(r)^4\Big)^2
\end{aligned}
\tag{A.0.5}
$$

doi:10.6342/NTU202302515

$$
\begin{aligned}
a_{11}(r) =& -4(\eta-2)\eta^2 r^2 e^{A(r)} B(r) B'(r) \\
& \Bigg(-2\gamma(\eta-2)(2\eta-1) r^2 B'(r)^2 \\
& + 2B(r)^2 \left(\gamma(\eta-4) r B'(r) - 2\left(\gamma(\eta+1)^2 - 3\alpha\eta^2\right)\right) \\
& + 2\gamma r B(r) \left((\eta-2)\eta r B''(r) - \left(2\eta^2+\eta-4\right) B'(r)\right) \\
& + B(r)^3 \left(4\gamma(\eta(\eta+2)+2) + 3\eta^2\left(r^2-4\alpha\right)\right) - 4\gamma B(r)^4 \Bigg)^2
\end{aligned}
\tag{A.0.6}
$$

$$
\begin{aligned}
b_{31}(r) =& 96\gamma(\eta-2)\eta^5 r^3 e^{A(r)} B(r)^4 \\
& \left(-4\alpha(\eta-2) r B'(r) + B(r)^2 \left(3(\eta-1) r^2 - 4\alpha(\eta-2)\right) + 4\alpha(\eta-2) B(r) \right)
\end{aligned}
\tag{A.0.7}
$$

$$
b_{23}(r) = -32\gamma^2(\eta-2)^3\eta^3(\eta+2) r^6 e^{A(r)} B(r)^3 \tag{A.0.8}
$$

doi:10.6342/NTU202302515

$$
\begin{aligned}
b_{22}(r) = & -16\gamma(\eta-2)\eta^2 r^4 e^{A(r)} B(r)^2 \\
& \Bigg(-\gamma(\eta-2)^2(\eta(11\eta+20)-12) r^2 B'(r)^2 \\
& + B(r)^2 \Big(24\alpha\left(\eta^2-4\right)\eta^2 + 2\gamma\left(\eta^3-28\eta+48\right) r B'(r) \\
& \qquad + \gamma(\eta(\eta(21-2\eta(4\eta+9))+88)+48) \Big) \\
& - 4\gamma(\eta-2)(\eta+3)\left(2\eta^2+\eta-4\right) r B(r) B'(r) \\
& + 2B(r)^3 \left(\gamma(\eta(\eta(\eta(4\eta+5)+5)-32)-48) + 3\left(\eta^2-4\right)\eta^2\left(r^2-4\alpha\right)\right) \\
& + \gamma((\eta-24)\eta+48) B(r)^4 \Bigg)
\end{aligned}
\tag{A.0.9}
$$

doi:10.6342/NTU202302515

$$
\begin{aligned}
b_{21}(r) = &-8\eta r^2 e^{A(r)} B(r) \\
&\Bigg(4\gamma^2(\eta-2)^3(2\eta-1)(\eta(5\eta+11)-6) r^4 B'(r)^4 \\
&+ 4\gamma^2(\eta-2)^2\left(2\eta^2+\eta-4\right)(\eta(7\eta+22)-12) r^3 B(r) B'(r)^3 \\
&+ 4B(r)^4 \Bigg(36\alpha^2\left(\eta^2-4\right)\eta^4 + 6\alpha\gamma(\eta(\eta(-6(\eta-1)\eta-19)+64)+32)\eta^2 \\
&\quad + \gamma r B'(r) \Big(-\gamma(\eta-2)(\eta(\eta(5\eta-71)+192)-144) r B'(r) \\
&\quad\quad - \gamma(\eta(\eta(\eta(8\eta(\eta(\eta+3)+6)-187)-396)+336)+576) \\
&\quad\quad + 3(\eta-2)\eta^2 \\
&\quad\quad \left(\left((16\eta-27)\eta^2+16\right) r^2 - 8\alpha\left((2\eta-11)\eta^2+16\right)\right) \Big) \\
&\quad + 2\gamma^2(\eta+1)^2(\eta(\eta(2\eta(\eta+3)-3)-40)-24) \Bigg) \\
&+ B(r)^6 \Bigg(4\gamma^2(\eta-4)(\eta(9\eta-40)+48) r B'(r) \\
&\quad + 8\gamma^2(\eta(\eta(\eta(\eta(2\eta(\eta+1)+17)+40)-22)-192)-144) \\
&\quad + 12\gamma\eta^2 \Big(\left(\eta\left(\eta\left(2\eta^2+\eta+9\right)-16\right)-32\right) r^2 \\
&\quad - 2\alpha\left(\eta\left(\eta\left(4\eta^2+2\eta+17\right)-16\right)-96\right) \Big) \\
&\quad + 9\left(\eta^2-4\right)\eta^4\left(r^2-4\alpha\right)^2 \Bigg) + b_{21,continue}(r) \Bigg)
\end{aligned}
\tag{A.0.10}
$$

doi:10.6342/NTU202302515

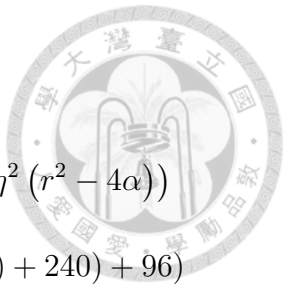

$$
\begin{aligned}
b_{21,continue}(r) =& 2B(r)^5\Big(6\gamma(\eta-4)rB'(r)\left(3\gamma\left(5\eta^2-16\right)+4(\eta-2)\eta^2\left(r^2-4\alpha\right)\right)\\
&+4\gamma^2(\eta(\eta(168-\eta(\eta(4\eta(\eta+3)+33)-8))+240)+96)\\
&-3\gamma\eta^2\Big(4\alpha(\eta(\eta(2(2-5\eta)\eta-41)+104)+96)\\
&+(\eta(\eta(10(\eta-2)\eta+27)-56)-32)r^2\Big)\\
&+36\alpha\left(\eta^2-4\right)\eta^4\left(r^2-4\alpha\right)\Big)\\
&+12\gamma(\eta-2)r^2B(r)^2B'(r)^2\\
&\Big(-2\alpha(\eta-2)(\eta(19\eta+12)-8)\eta^2\\
&-\gamma(\eta-4)(\eta-2)(\eta(\eta+8)-4)rB'(r)\\
&+\gamma\left(\eta\left(\eta\left(\eta\left(6\eta^2+20\eta-15\right)-87\right)-16\right)+48\right)\Big)\\
&-2\gamma rB(r)^3B'(r)\\
&\Big(-24\alpha(\eta-2)(\eta(\eta(5\eta-28)+4)+16)\eta^2\\
&+(\eta-2)rB'(r)\\
&\Big(4\gamma(\eta(\eta(\eta(\eta(7\eta+8)+19)-111)-120)+144)\\
&+3\left(7\eta^3-36\eta+16\right)\eta^2\left(r^2-4\alpha\right)\Big)\\
&-2\gamma(\eta+4)\left(2\eta^2+\eta-4\right)\left(\eta\left(4\eta^2+2\eta-17\right)-12\right)\Big)\\
&+2\gamma B(r)^7\Big(4\gamma(\eta(\eta(\eta(5\eta-8)-32)+16)+96)\\
&\qquad+3(\eta(5\eta-24)+32)\eta^2\left(r^2-4\alpha\right)\Big)\\
&-8\gamma^2(\eta(7\eta-24)+24)B(r)^8
\end{aligned}
\tag{A.0.11}
$$

$$
b_{16}(r) = 16(\eta-2)^3(\eta(3\eta+8)-4)r^6e^{A(r)}(\gamma-2\gamma\eta)^2 \tag{A.0.12}
$$

doi:10.6342/NTU202302515

$$
\begin{aligned}
b_{15}(r) = & -32\gamma^2(\eta-2)^2(2\eta-1)r^5 e^{A(r)}B(r) \\
& \left((\eta-4)(\eta(\eta+13)-6)B(r) - 3\left(2\eta^2+\eta-4\right)(\eta(\eta+4)-2)\right)
\end{aligned}
\tag{A.0.13}
$$

$$
\begin{aligned}
b_{14}(r) = & -16\gamma(\eta-2)r^4 e^{A(r)}B(r)^2 \\
& \Bigg(3\Bigg(4\alpha(\eta-2)(2\eta-1)(\eta(9\eta+10)-4)\eta^2 \\
& \quad + \gamma(80-\eta(\eta(\eta(4\eta(3\eta+14)-43)-242)+53)+200))\Bigg) \\
& + B(r)\Bigg(\gamma(\eta(\eta(17(\eta-12)\eta+653)-776)+240)B(r) \\
& \quad + 2\gamma(\eta(\eta(\eta(\eta(12\eta(\eta+1)+67)-345)-231)+688)-240) \\
& \quad + 3(\eta-2)(2\eta-1)(\eta(3\eta+8)-4)\eta^2\left(r^2-4\alpha\right)\Bigg)\Bigg)
\end{aligned}
\tag{A.0.14}
$$

doi:10.6342/NTU202302515

$$
\begin{aligned}
b_{13}(r) =& 16\gamma r^3 e^{A(r)} B(r)^3 \\
&\Bigg(12\alpha(\eta-2)(\eta(5\eta(\eta(2\eta-19)+6)+88)-32)\eta^2 \\
&+ B(r)\Bigg(B(r)\Big(2\gamma(\eta-4)(\eta(\eta(21\eta-107)+176)-80)B(r) \\
&\qquad - 2\gamma(\eta(\eta(\eta(2\eta((\eta-2)\eta-67)+551)+140)-1808)+960) \\
&\qquad - 3(\eta-4)(\eta-2)((\eta-18)\eta+8)\eta^2\left(r^2-4\alpha\right)\Big) \\
&- 2\gamma(4\eta^7+40\eta^6+140\eta^5-485\eta^4-923\eta^3+1340\eta^2+1264\eta-960) \\
&+ 3(\eta-2)\eta^2\Big((\eta(\eta(5\eta(6\eta-13)-6)+84)-32)r^2 \\
&\qquad - 8\alpha((\eta-10)\eta+4)\left(3\eta^2+\eta-8\right)\Big)\Bigg) \\
&+ 2\gamma\left(2\eta^2+\eta-4\right)(\eta(\eta(2\eta(\eta(3\eta+22)-11)-189)-40)+80)\Bigg)
\end{aligned}
\tag{A.0.15}
$$

doi:10.6342/NTU202302515

$$
\begin{aligned}
b_{12}(r) =& \frac{4r^2 e^{A(r)} B(r)^4}{\eta - 2} \\
& \Bigg(12 \Bigg(12\alpha^2 (\eta-2)^2 (3\eta(\eta+4) - 4)\eta^4 \\
& \quad - 12\alpha\gamma(\eta-2)\left(\eta\left(\eta\left(2\eta\left(\eta^2+\eta+16\right)-77\right)-32\right)+32\right)\eta^2 \\
& \quad + \gamma^2(4\eta^8 + 80\eta^7 + 4\eta^6 - 346\eta^5 - 235\eta^4 + 764\eta^3 + 712\eta^2 - 320\eta - 320) \Bigg) \\
& + B(r) \Bigg(B(r) \Big(4\gamma B(r) \big(\gamma(\eta(\eta((\eta(77\eta - 548) + 1544)\eta - 1984) + 960)B(r) \\
& + 2\gamma(28\eta^6 - 109\eta^5 - 124\eta^4 + 784\eta^3 + 96\eta^2 - 2496\eta + 1920) \\
& + 3(\eta-2)(\eta(\eta(14\eta - 81) + 160) - 96)\eta^2 \left(r^2 - 4\alpha\right) \big) \\
& + 8\gamma^2 \\
& (6\eta^8 - 16\eta^7 + 86\eta^6 + 147\eta^5 \\
& - 949\eta^4 - 988\eta^3 + 3192\eta^2 + 1536\eta - 2880) \\
& + 24\gamma(\eta-2)\eta^2 \big((\eta(\eta(\eta(3\eta(\eta+1)+10) - 4) - 140) + 96)r^2 \\
& - 2\alpha\left(\eta\left(\eta\left(2\eta\left(3\eta^2+\eta+20\right)+3\right)-416\right)+288\right) \big) \\
& + 9(\eta-2)^2(\eta(3\eta+8) - 4)\eta^4 \left(r^2 - 4\alpha\right)^2 \Big) \\
& + 4 \Big(\gamma^2 \\
& (-24\eta^8 - 56\eta^7 - 368\eta^6 + 962\eta^5 + 2928\eta^4 \\
& - 2432\eta^3 - 7168\eta^2 + 896\eta + 3840) \\
& - 3\gamma(\eta-2)\eta^2 \Big(3(\eta(\eta(2\eta(\eta(3\eta - 11) + 19) - 39) - 40) + 32)r^2 \\
& - 4\alpha\left(\eta\left(\eta\left(2\eta\left(8\eta^2 - 4\eta + 83\right) - 309\right) - 352\right) + 288\right) \Big) \\
& + 18\alpha(\eta-2)^2(\eta(3\eta+10) - 4)\eta^4 \left(r^2 - 4\alpha\right) \Big) \Big) \Big)
\end{aligned}
\tag{A.0.16}
$$

doi:10.6342/NTU202302515

$$
\begin{aligned}
b_{11}(r) =& \frac{8re^{A(r)}B(r)^5}{\eta-2} \\
& \Bigg(24\Bigg(12\alpha^2(\eta-2)(5\eta-4)\eta^4 \\
& -\alpha\gamma\left(\eta\left(\eta\left(\eta\left(4\eta^2+42\eta-61\right)-212\right)+96\right)+128\right)\eta^2 \\
& +\gamma^2(\eta+1)^2\left(2\eta^2+\eta-4\right)\left(\eta\left(2\eta^2+\eta-12\right)-8\right)\Bigg) \\
& +B(r)\Bigg(B(r)\Bigg(B(r)\big(2\gamma B(r)(4\gamma(\eta-4)(\eta(11\eta-32)+24)B(r) \\
& -4\gamma(\eta(\eta(\eta(\eta(13\eta-42)-63)+160)+296)-480) \\
& -3(\eta-4)(\eta(13\eta-40)+32)\eta^2\left(r^2-4\alpha\right)) \\
& +16\gamma^2(\eta(\eta(\eta(\eta((\eta-2)\eta(\eta+10)-80)+115)+348)-168)-480) \\
& +6\gamma\eta^2\big((\eta(\eta(\eta(2\eta(2\eta-9)+33)-108)+368)-384)r^2 \\
& -8\alpha(\eta((\eta-4)\eta(\eta(2\eta+5)+6)+240)-256)\big) \\
& +9(\eta-4)(\eta-2)^2\eta^4\left(r^2-4\alpha\right)^2\Big) \\
& +2\big(-8\gamma^2(6\eta^7+88\eta^6+80\eta^5-464\eta^4-719\eta^3+332\eta^2+1096\eta+480) \\
& +3\gamma\eta^2\big(8\alpha(\eta(\eta(\eta(\eta(2\eta-27)-49)+196)+144)-384) \\
& +(384-\eta(\eta(\eta(16\eta-69)+108)+160))r^2\big) \\
& -9(\eta-2)\eta^4\left(r^2-4\alpha\right)\left((\eta(4\eta-7)+4)r^2-4\alpha((\eta-11)\eta+12)\right)\big)\Big) \\
& -8\gamma^2(\eta(\eta(\eta(2\eta(\eta(\eta(3\eta+44)+40)-232)-719)+332)+1096)+480) \\
& +6\gamma\eta^2\Big(8\alpha(\eta-2)(\eta(\eta(\eta(2\eta+49)+96)-88)-128) \\
& +\left(\eta\left(\eta\left(\eta\left(2\eta\left(-6\eta^2+8\eta+1\right)-41\right)+124\right)-16\right)-128\right)r^2\Big) \\
& +72\alpha(\eta-2)\eta^4\left(2\alpha((\eta-26)\eta+24)-((\eta-12)\eta+8)r^2\right)\Big)\Big)
\end{aligned}
\tag{A.0.17}
$$

doi:10.6342/NTU202302515

$$
\begin{aligned}
c_{00}(r) = &- e^{A(r)} \\
&\Bigg(16\eta\Big(B(r)^3\Big(4\gamma(\eta(\eta+2)+2)+3\eta^2\left(r^2-4\alpha\right)\Big) \\
&-4B(r)^2\left(\gamma(\eta+1)^2-3\alpha\eta^2\right)-4\gamma B(r)^4\Big) \\
&\Big(2B(r)^7\left(4\gamma(\eta(\eta+2)+2)+3\eta^2\left(r^2-4\alpha\right)\right) \\
&+B(r)^5\left(-8\gamma(\eta+1)^2(\eta(\eta+2)+2)-6\eta^2\left(((\eta-1)\eta+1)r^2-4\alpha(2\eta+3)\right)\right) \\
&+8(\eta+1)B(r)^4\left(\gamma(\eta+1)^3-6\alpha\eta^2\right)-8\gamma B(r)^8\Big) \\
&+\frac{1}{\eta-2}\Bigg(\Big(B(r)^5\big(-8\gamma\left(\eta^3-5\eta-12\right)-6(\eta-4)\eta^2\left(r^2-4\alpha\right)\big) \\
&+B(r)^4\left(8\gamma\left(2(\eta+3)\eta^3-13\eta-12\right)-6\eta^2\left(8\alpha(3\eta-4)+(\eta(4\eta-7)+4)r^2\right)\right) \\
&+2B(r)^3\left(12\alpha\eta^2(5\eta-4)-4\gamma(\eta+1)^2\left(2\eta^2+\eta-4\right)\right)+8\gamma(\eta-4)B(r)^6\Big)^2\Bigg) \\
&+2\eta\Big(-2rB(r)\Big(-12(\eta-4)\eta^2rB(r)^5-12\eta^2(\eta(4\eta-7)+4)rB(r)^4\Big) \\
&\Big(B(r)^3\big(4\gamma(\eta(\eta+2)+2) \\
&+3\eta^2\left(r^2-4\alpha\right)\big)-4B(r)^2\left(\gamma(\eta+1)^2-3\alpha\eta^2\right)-4\gamma B(r)^4\Big) \\
&+12\eta^2r^2B(r)^4\Big(B(r)^5\left(-8\gamma\left(\eta^3-5\eta-12\right)-6(\eta-4)\eta^2\left(r^2-4\alpha\right)\right) \\
&+B(r)^4\left(8\gamma\left(2(\eta+3)\eta^3-13\eta-12\right)-6\eta^2\left(8\alpha(3\eta-4)+(\eta(4\eta-7)+4)r^2\right)\right) \\
&+2B(r)^3\left(12\alpha\eta^2(5\eta-4)-4\gamma(\eta+1)^2\left(2\eta^2+\eta-4\right)\right)+8\gamma(\eta-4)B(r)^6\Big) \\
&+2B(r)\Big(B(r)^3\left(4\gamma(\eta(\eta+2)+2)+3\eta^2\left(r^2-4\alpha\right)\right) \\
&-4B(r)^2\left(\gamma(\eta+1)^2-3\alpha\eta^2\right)-4\gamma B(r)^4\Big) \\
&\Big(B(r)^5\big(-8\gamma\left(\eta^3-5\eta-12\right)-6(\eta-4)\eta^2\left(r^2-4\alpha\right)\big) \\
&+B(r)^4\left(8\gamma\left(2(\eta+3)\eta^3-13\eta-12\right)-6\eta^2\left(8\alpha(3\eta-4)+(\eta(4\eta-7)+4)r^2\right)\right) \\
&+2B(r)^3\left(12\alpha\eta^2(5\eta-4)-4\gamma(\eta+1)^2\left(2\eta^2+\eta-4\right)\right)+8\gamma(\eta-4)B(r)^6\Big)\Big)\Bigg)
\end{aligned}
\tag{A.0.18}
$$

doi:10.6342/NTU202302515

Appendix B

Results of Time Dependent Simulation

In this appendix, we show plots of the time dependent result with the setup mentioned in chapter 7. The figures show the time slices of the result. Their time order are assumed to be first from left to right and then from top to bottom in the same page, and after the time order continues to the proceeding page. This set of figures start from the initial condition and end at the final state shown in chapter 7. For better quality of the figures, we are posting them from the next page.

doi:10.6342/NTU202302515

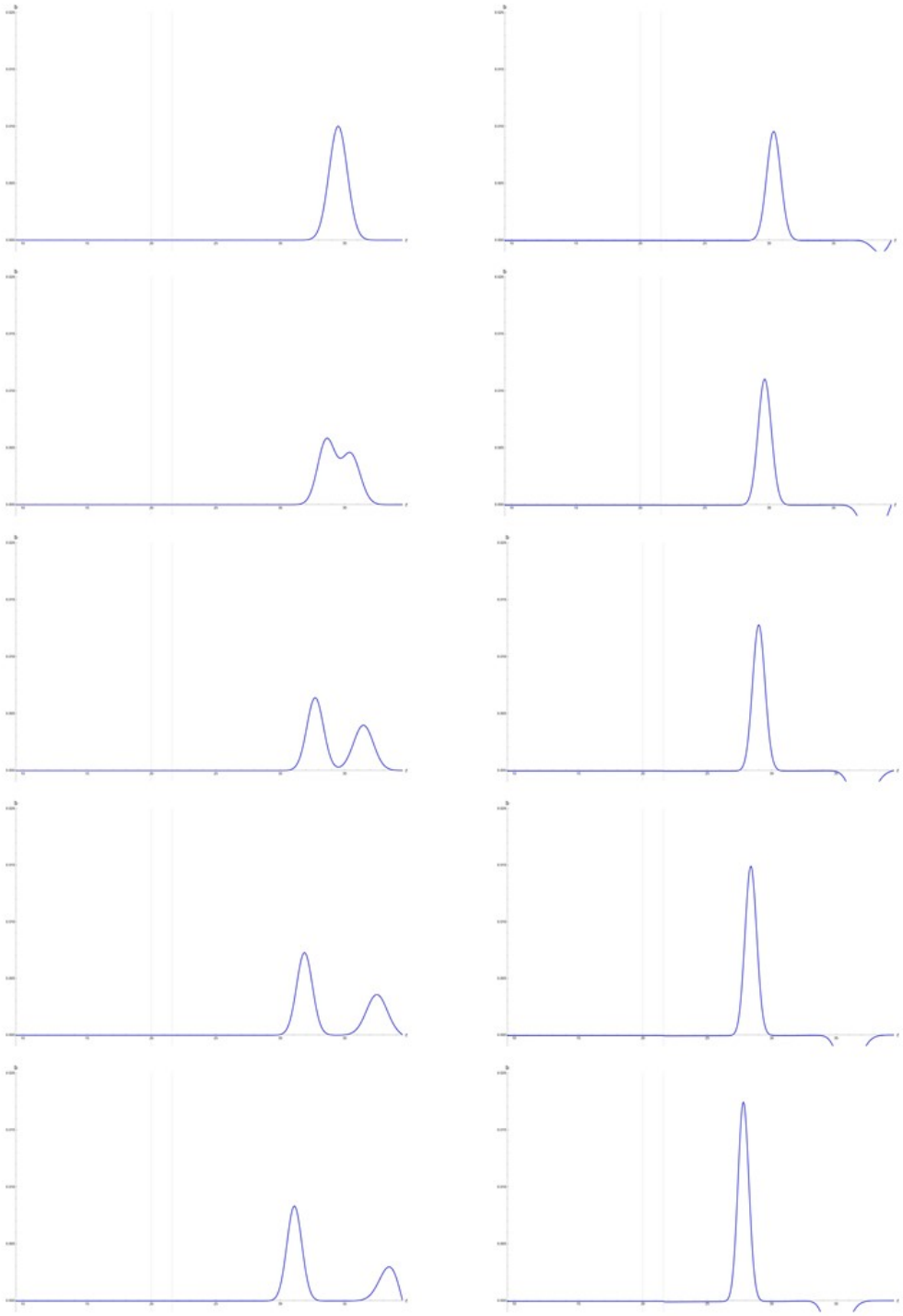

Figure B.1: Result of simulation (1/6).

doi:10.6342/NTU202302515

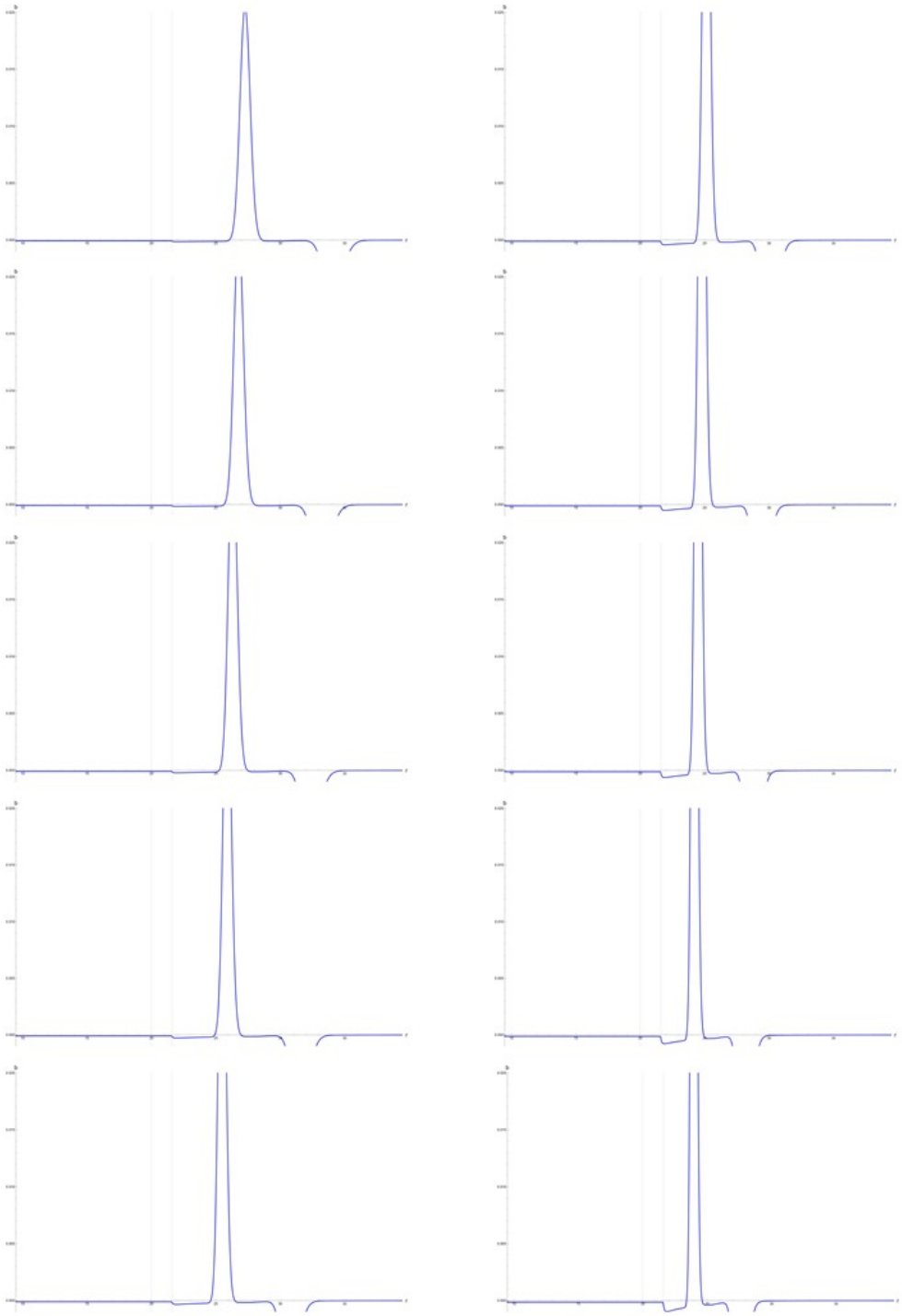

Figure B.2: Result of simulation (2/6).

doi:10.6342/NTU202302515

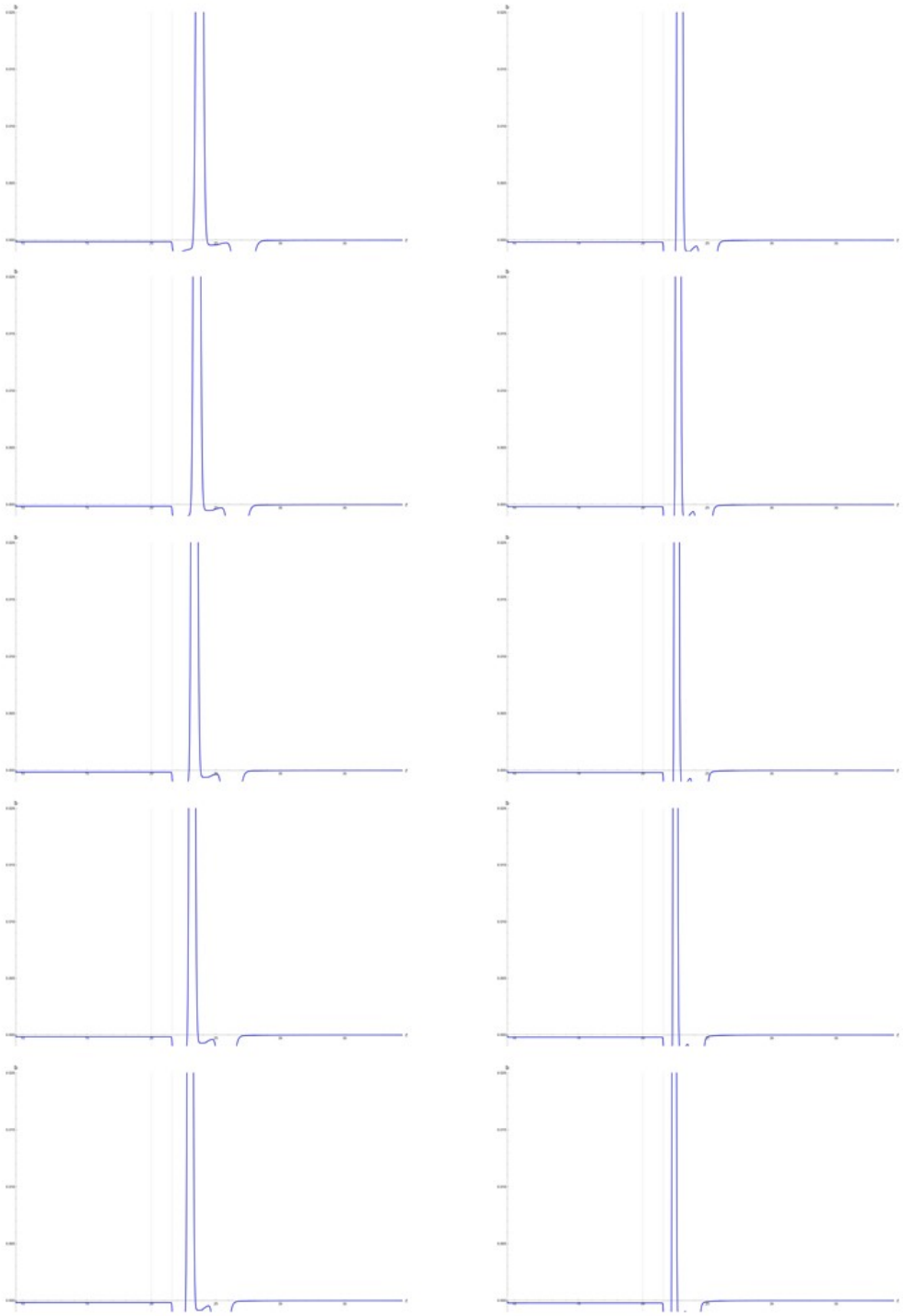

Figure B.3: Result of simulation (3/6).

doi:10.6342/NTU202302515

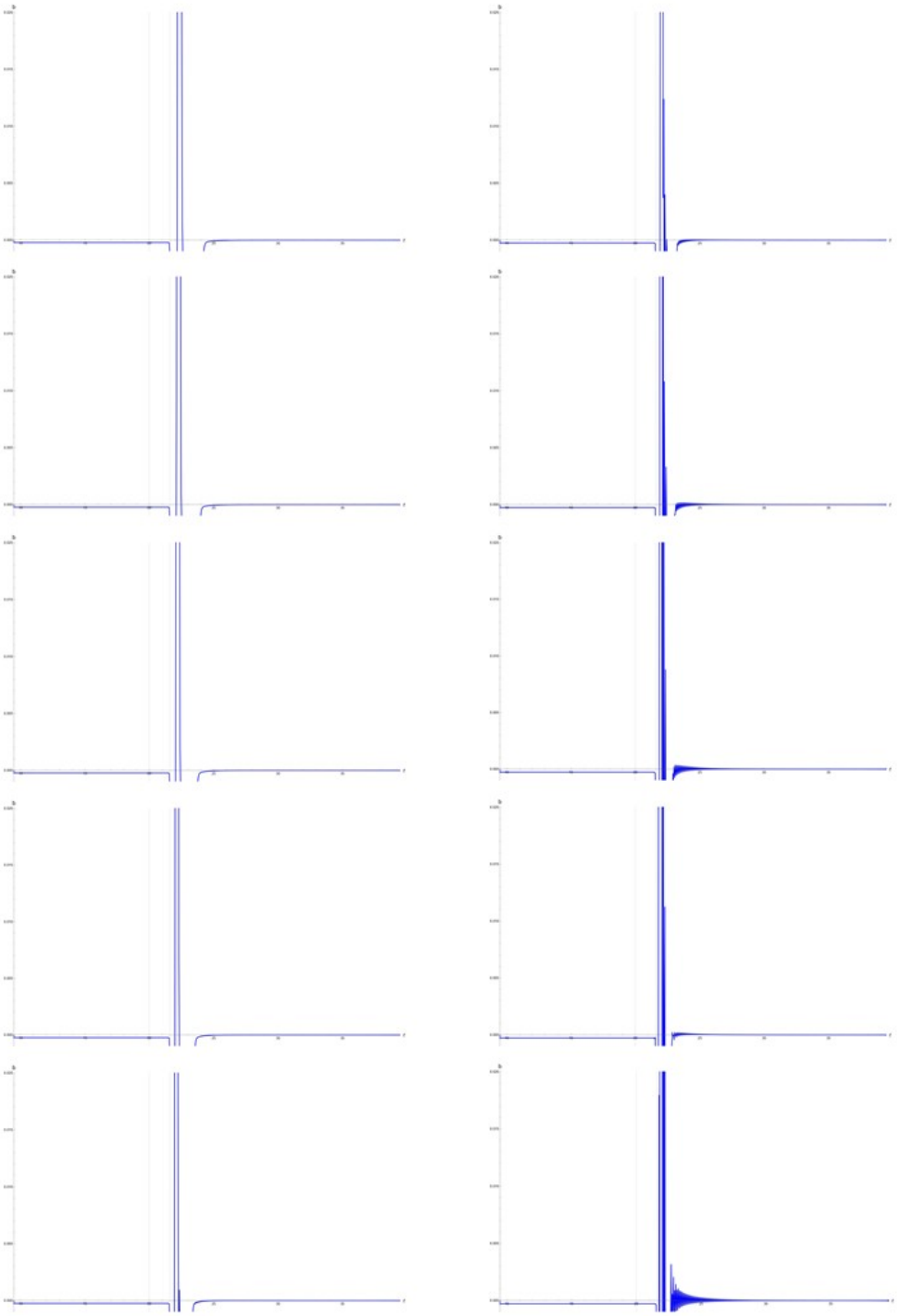

Figure B.4: Result of simulation (4/6).

doi:10.6342/NTU202302515

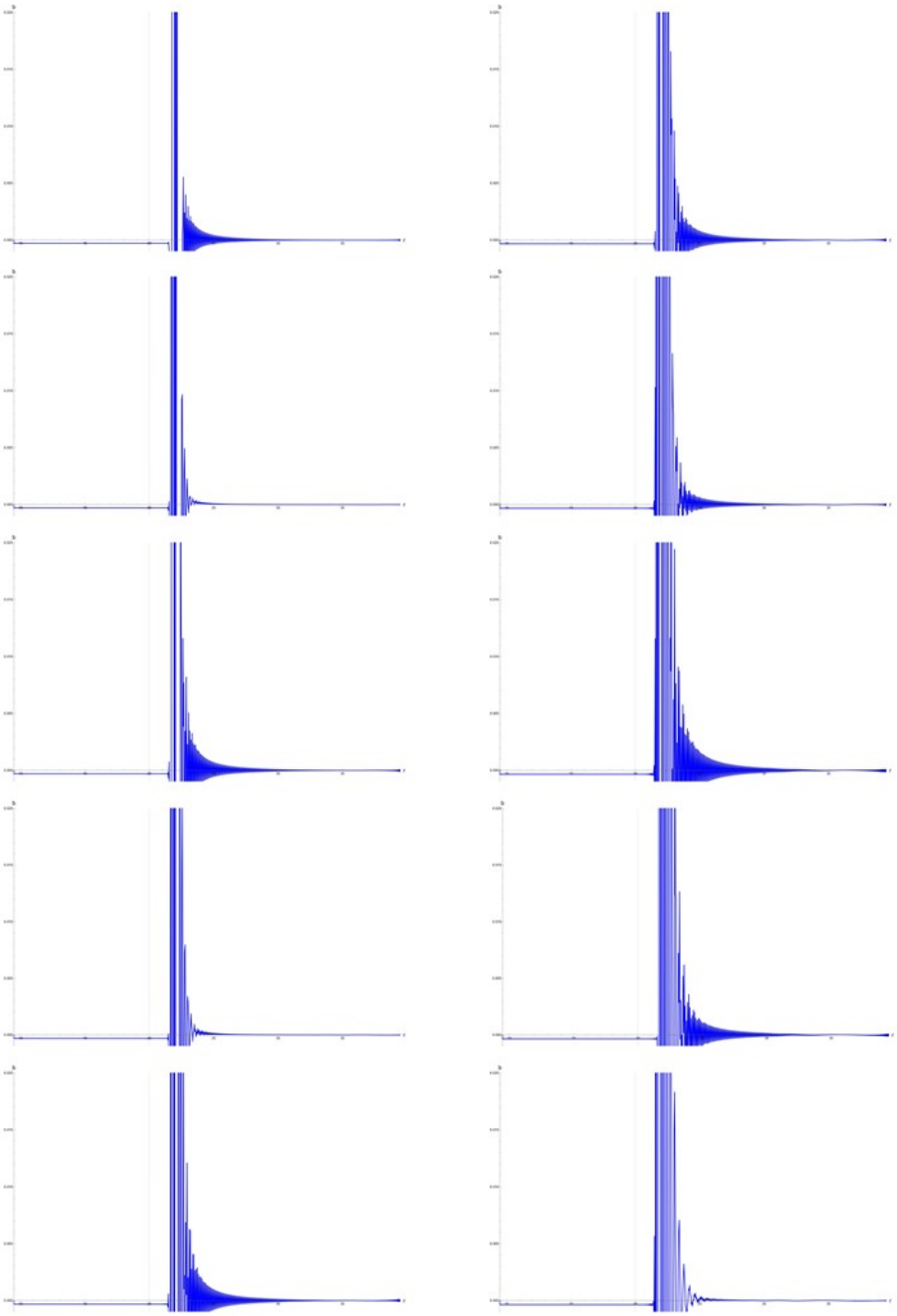

Figure B.5: Result of simulation (5/6).

doi:10.6342/NTU202302515

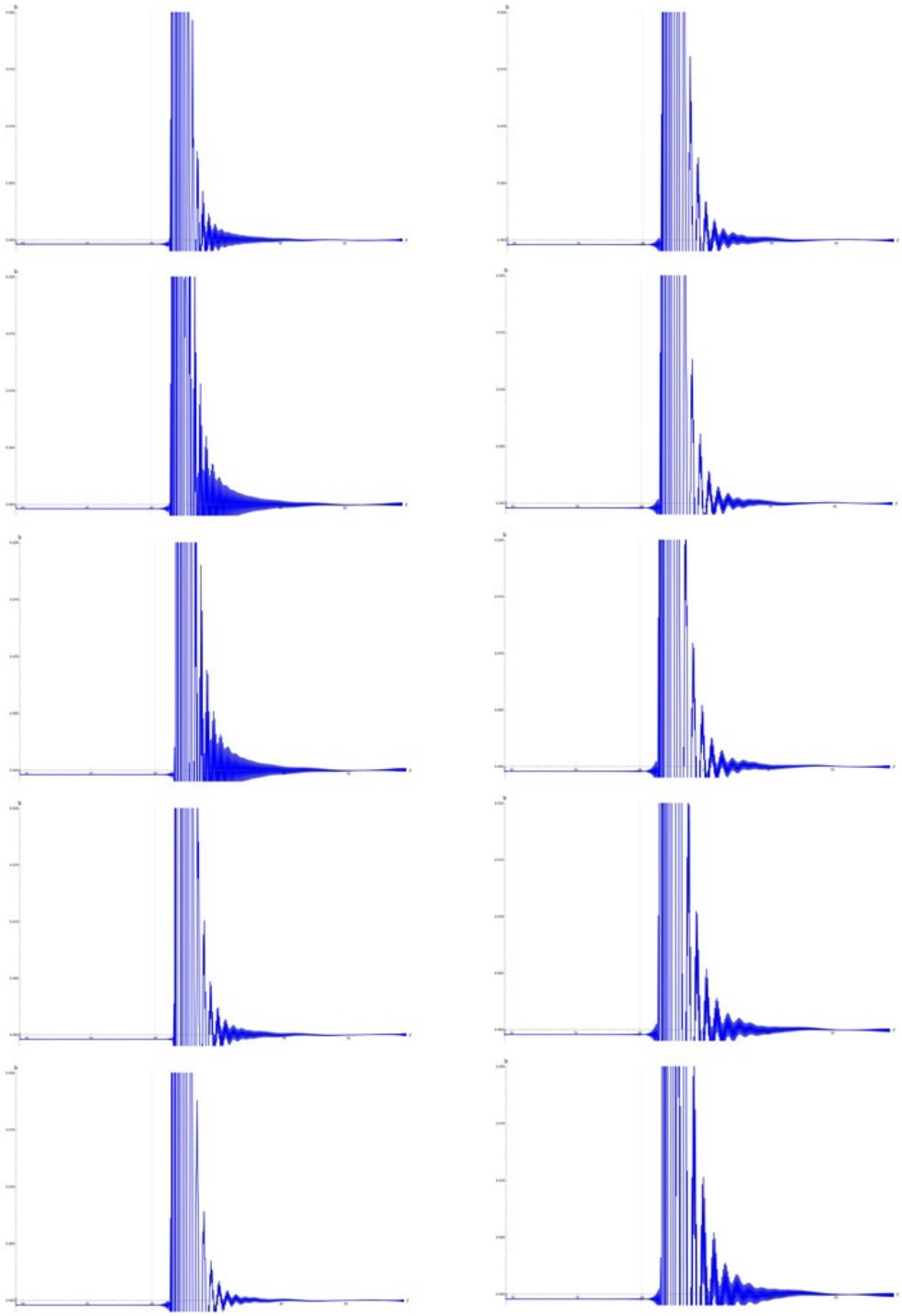

Figure B.6: Result of simulation (6/6).

doi:10.6342/NTU202302515

doi:10.6342/NTU202302515